Physical properties of *Herschel* selected galaxies in a semi-analytic galaxy formation model

Sami-Matias Niemi[1,2]⋆, Rachel S. Somerville[1,3], Henry C. Ferguson[1],
Kuang-Han Huang[3], Jennifer Lotz[1] and Anton M. Koekemoer[1]

[1]*STScI, 3700 San Martin Drive, Baltimore, MD 21218, United States*
[2]*University of Turku, Department of Physics and Astronomy, Tuorla Observatory, Väisäläntie 20, Piikkiö, Finland*
[3]*Department of Physics and Astronomy, Johns Hopkins University, Baltimore, MD 21218, United States*

arXiv:1201.2410v1 [astro-ph.CO] 11 Jan 2012

ABSTRACT
We make use of a semi-analytic cosmological model that includes simple prescriptions for dust attenuation and emission to make predictions for the observable and physical properties of galaxies that may be detected by the recently launched *Herschel* Space Observatory in deep fields such as GOODS-*Herschel*. We compare our predictions for differential galaxy number counts in the *Herschel* PACS (100 and 160 μm) and SPIRE (250, 350, and 500 μm) bands with available observations. We find very good agreement with the counts in the PACS bands, for the overall counts and for galaxies binned by redshift at $z < 2$. At $z > 2$ our model underpredicts the number of bright galaxies in the PACS bands by a factor of ten. The agreement is much worse for all three SPIRE bands, and becomes progressively worse with increasing wavelength. We discuss a number of possible reasons for these discrepancies, and hypothesize that the effect of blending on the observational flux estimates is likely to be the dominant issue. We note that the PACS number counts are relatively robust to changes in the dust emission templates, at least for the three sets of templates that we have tested, while the predicted SPIRE number counts are more template dependent especially at low redshift. We present quantitative predictions for the relationship between the observed PACS 160 and SPIRE 250 μm fluxes and physical quantities such as halo mass, stellar mass, cold gas mass, star formation rate, and total infrared (IR) luminosity, at different redshifts. We also present predictions for the radial sizes of *Herschel*-selected disks at high redshift ($z > 2$) and find reasonable agreement with the available observations. Finally, we present quantitative predictions for the correlation between PACS 160 μm flux and the probability that a galaxy has experienced a recent major or minor merger. Although our models predict a strong correlation between these quantities, such that more IR-luminous galaxies are more likely to be merger-driven, we find that a significant fraction (more than half) of all high redshift IR-luminous galaxies detected by *Herschel* are able to attain their high star formation rates without enhancement by a merger.

Key words: methods: numerical - galaxies: formation - galaxies: evolution - galaxies: mergers - galaxies: star formation - galaxies: infrared selected

1 INTRODUCTION

One of the most important discoveries from extragalactic observations in the mid- and far-infrared has been the identification of luminous and ultra-luminous infrared bright galaxies (LIRGs; $L_{IR} > 10^{11}L_\odot$ and ULIRGs; $L_{IR} > 10^{12}L_\odot$, respectively). These objects have been studied extensively in the literature (e.g. Rieke & Low 1972; Harwit et al. 1987; Sanders et al. 1988; Sanders, Scoville & Soifer 1991; Condon et al. 1991; Auriere et al. 1996; Duc, Mirabel & Maza 1997; Genzel et al. 1998; Lutz et al. 1998; Rigopoulou et al. 1999; Rowan-Robinson 2000; Genzel et al. 2001; Colina et al. 2001; Colbert et al. 2006; Dasyra et al. 2006b; Hernán-Caballero et al. 2009; Magdis et al. 2011), and found to emit more energy at infrared wavelengths ($\sim 5 - 500 \mu$m) than at all other wavelengths combined (e.g. Sanders & Mirabel 1996).

⋆ E-mail: sammy@sammyniemi.com (SMN)

Even though the luminous infrared galaxies are rare objects in the local Universe (e.g. Lagache, Puget & Dole 2005), reasonable assumptions about the lifetime of the infrared phase (see, e.g. Farrah et al. 2003, and references therein) suggest that a substantial fraction of all massive galaxies pass through a stage of intense infrared emission during their lifetime (Sanders & Mirabel 1996, and references therein). Consequently, the majority of the most luminous galaxies in the Universe emit the bulk of their energy in the far-infrared. Furthermore, LIRGs and ULIRGs dominate the cosmic star formation rate density at $z \sim 1 - 2$, accounting for 70 per cent of the star formation activity at these epochs (e.g. Floc'h et al. 2005). This makes the IR an extremely interesting wavelength regime to study, especially in the context of the cosmic star formation history, and galaxy formation and evolution.

Understanding IR bright galaxies is especially important because light from bright, young blue stars is often attenuated by dust (for a review see Calzetti 2001). The observed rest-frame ultra-violet (UV) light of a galaxy may therefore provide a biased view of the star formation rate in the galaxy. For example, the global star formation rate required to explain the far-infrared and submillimetre background appears to be higher than that inferred from the data in the UV-optical (e.g. Hughes et al. 1998, and references therein). The dust attenuated light from blue stars is however not lost, but is re-radiated at IR wavelengths. As a result, a large fraction of the radiation from star formation is radiated not at UV or optical but at IR rest-frame wavelengths.

The European Space Agency's *Herschel* Space Observatory (Pilbratt et al. 2010) was launched in May of 2009. It observes the Universe at infrared wavelengths, from 60 to 670 μm, and opens up a huge region of new parameter space for surveys in area, depth and wavelength. Consequently, a primary goal of *Herschel* is to explore the evolution of obscured galaxies. With *Herschel*, we can finally probe the IR light of high-redshift galaxies from 70 to 160 and 250 to 500 μm with the Photodetector Array Camera & Spectrometer (PACS; Poglitsch et al. 2010) and Spectral and Photometric Imaging Receiver (SPIRE; Griffin et al. 2010), respectively. Unfortunately, at such long wavelengths, contamination and crowding, rather than the depth of the observations, often becomes a limiting factor (e.g. Blain, Ivison & Smail 1998; Brisbin et al. 2010; Lacey et al. 2010). As a result, the interpretation of IR observations can be less than straightforward. This is especially true when probing galaxies at high redshift. Despite the potential complications, several deep *Herschel* observations have been performed (e.g. Oliver et al. 2010) since the launch of the observatory and more will likely follow.

Early *Herschel* observations and studies have already generated some very interesting results, such as the conclusions that the majority of the detected high-redshift galaxies are large and massive spiral galaxies (e.g. Cava et al. 2010) with extremely high star formation rates (e.g. Brisbin et al. 2010). Furthermore, the minimum dark matter halo mass of IR bright galaxies was recently constrained to be about $3 \times 10^{11} M_\odot$ (Amblard et al. 2011), while the average dust temperature of H-ATLAS sources was found to be 28 ± 8 K (Amblard et al. 2010). However, because of the very large beam of the *Herschel* telescope and the difficulty of making unique associations between optically detected galaxies and the PACS or SPIRE sources, many open questions about the physical nature of the populations detected by *Herschel* remain: for example, what are their stellar masses, sizes, and morphologies (spheroid or disk dominated)? Are they dynamically relaxed galaxies, or interacting or merging systems?

One can turn to theoretical modelling to aid in the interpretation of these observations, and to make predictions about the nature of the objects that *Herschel* should detect at various redshifts. In the IR, all the theoretical models in the literature can be divided into two broad classes: *phenomenological* models and *cosmological* models. The phenomenological models (sometimes called "backwards evolution" models) are based on observed luminosity functions, and assume simple functional forms to describe the evolution of galaxy luminosity functions or SFR with redshift. Template spectral energy densities (SEDs) based on observed galaxies are used to transform between different wavelengths (e.g. Dale et al. 2001; Dale & Helou 2002; Lagache, Dole & Puget 2003). In contrast, in semi-analytic cosmological models, the evolution of galaxy properties is predicted based on the framework of the hierarchical structure formation, or Cold Dark Matter (CDM) theory. In these simulations, the evolution of structure in the dark matter component is characterized via "merger trees", and simplified prescriptions are used to model the main physical processes such as cooling and accretion of gas, star formation, chemical evolution, stellar, supernovae and active galactic nuclei feedback (e.g. Croton et al. 2006; Somerville et al. 2008). Based on the resulting predicted star formation and chemical enrichment histories, the SED for unattenuated light from stars (which dominates the SED shortwards of about 3 μm) may be calculated using stellar population synthesis models (e.g. Tinsley & Gunn 1976; Worthey 1994; Leitherer & Heckman 1995; Bruzual & Charlot 2003; Maraston 2005; Conroy, Gunn & White 2009, and references therein).

Modelling the impact of dust attenuation, and computing the SED of the dust emission, are less straightforward. A standard assumption is that all energy absorbed by dust is re-radiated. One can then break the problem into two parts: computing the amount of light absorbed (and scattered) by dust as a function of wavelength, and computing the amount of re-radiated light emitted by dust as a function of wavelength. One approach is to couple the semi-analytic models with a radiative transfer (RT) code (Granato et al. 2000; Baugh et al. 2005a; Fontanot et al. 2007; Lacey et al. 2008, 2010) to compute the dust attenuation and scattering, and a detailed dust model, that assumes a specific dust composition and set of grain properties, to compute the dust emission SEDs. Another approach is to use analytic models relating the attenuation to the column density of dust (assumed to be traced by metals in the cold gas) in galactic disks (e.g. Guiderdoni & Rocca-Volmerange 1987). To compute the dust emission SED, one can then use empirical dust SED templates based on analytic dust models calibrated to observations, or observed galaxies (Guiderdoni et al. 1998; Devriendt, Guiderdoni & Sadat 1999; Devriendt & Guiderdoni 2000).

The former approach (full RT+dust model) has the clear advantage of providing more detailed and accurate predictions of the galaxy SEDs, given the input assump-

tions, and certainly provides a better estimate of galaxy-to-galaxy scatter in the SED properties. It has the disadvantage of being computationally quite expensive, and perhaps not merited given that semi-analytic models do not provide detailed information about the relative geometry of stars and dust in galaxies, nor about the composition or properties of the dust, which may vary with cosmic time or environment. Fontanot et al. (2009b) and Fontanot & Somerville (2010) have shown that the analytic recipes for predicting dust attenuation and the empirical template approach for dust emission provide reasonably good agreement, in most cases, with statistical quantities such as galaxy luminosity functions and counts as computed with the full RT approach using the GRASIL code (Silva et al. 1998). Moreover, this analytic approach to dust attenuation and emission was adopted by Somerville et al. (2011, hereafter S11) and Gilmore et al. (2011), who showed that it provided good agreement with observed galaxy luminosity functions for rest-UV to NIR wavelengths and redshifts $0 < z < 4$. This approach also produced fairly good agreement with observational estimates of the *total* IR luminosity function at $0 < z < 2$, and with the observed Extragalactic Background Light. However, these models produced poorer agreement at longer wavelengths ($\lambda \gtrsim 8\mu m$), particularly for luminous higher redshift ($z \gtrsim 2$) galaxies. Thus, the limitations of our approach should be kept in mind. Part of the goal of this work is to determine where improvements to this kind of analytic approach must be made by confronting the models with recent observations from Herschel.

In this work we use the SAM introduced in Somerville & Primack (1999), with significant updates as presented by Somerville et al. (2008), Hopkins et al. (2009), and S11, and undertake a study of galaxies that should be detected by current *Herschel* surveys both locally and at high redshift. We focus on the populations that can be detected in the relatively deep surveys being carried out with *Herschel*, in particular the GOODS-*Herschel* project (PI D. Elbaz). The redshift range $2 \leq z < 4$ is of special interest because 1) it spans the peak of the cosmic star formation activity in the Universe 2) it probes what are probably the earliest epochs for which individual galaxies can be detected with *Herschel* and 3) many open questions remain about the nature of galaxy populations, especially luminous IR galaxies, at these epochs.

This paper is organised as follows. In Section 2, we provide a brief overview of the semi-analytic galaxy formation model used in our study, the model for dust attenuation and emission, how we construct our mock light cone, and our sample selection criteria. In Section 3 we present our predictions for observable properties of *Herschel* galaxies such as counts and luminosity functions. In Section 4, we show predictions for the physical properties of *Herschel*-selected galaxies at different redshifts. Finally we summarise our results and conclude in Section 5.

2 THE SEMI-ANALYTIC MODEL

2.1 The Semi-analytic Galaxy Formation Model

We compute the formation and evolution of galaxies within the ΛCDM cosmology using the semi-analytic galaxy formation model (SAM) introduced in Somerville & Primack

(1999) and described in detail in Somerville et al. (2008), hereafter S08. Our model also includes the modified recipe for bulge formation and starburst efficiency described in Hopkins et al. (2009). In summary, the S08 SAM includes the following physically motivated recipes: 1) growth of structure in the dark matter component in a hierarchical clustering framework, as characterized by "merger trees"; 2) the shock heating and radiative cooling of gas; 3) conversion of cold gas into stars according to an empirical "Kennicutt-Schmidt" relation; 4) the evolution of stellar populations; 5) feedback and metal enrichment of the Interstellar (ISM) and Intracluster Medium (ICM) from supernovae explosions; 6) two modes ("quasar" and "radio" mode) of black hole growth and feedback from active galactic nuclei; 7) starbursts and morphological transformation by galaxy mergers. The SAM can be used to predict physical quantities such as stellar and cold gas masses and metallicities of galaxies, their star formation and merger histories, and their luminosities and sizes.

The merging histories (or merger trees) of dark matter haloes are constructed based on the Extended Press-Schechter formalism using the method described in Somerville & Kolatt (1999), with improvements described in S08. These merger trees record the growth of dark matter haloes via merging and accretion, with each "branch" representing a merger of two or more haloes. In this work we follow each branch back in time to a minimum progenitor mass of $10^9 M_\odot$. This mass scale is sufficient to resolve the formation histories of the relatively bright, massive galaxies that we study in this work, which occupy halos with masses greater than a few $\times 10^{11} M_\odot$.

In the SAM of S08 the star formation occurs in two modes, a "quiescent" mode in isolated disks, and a merger-driven "starburst" mode. Star formation in isolated disks is modelled using the empirical Kennicutt-Schmidt relation (Kennicutt 1989), assuming that only gas above a fixed critical surface density is eligible to form stars. The efficiency and timescale of the merger driven burst mode is a function of merger ratio and the gas fractions of the progenitors, and is based on the results of hydrodynamic simulations (Robertson et al. 2006; Hopkins et al. 2009).

In this work we have assumed a standard ΛCDM universe and a Chabrier stellar initial mass function (IMF; Chabrier 2003). We adopt the following cosmological parameter values: $\Omega_m = 0.28$, $\Omega_\Lambda = 0.72$, $H_0 = 70.0$, $\sigma_8 = 0.81$ and $n_s = 0.96$, which are consistent with the five year Wilkinson Microwave Anisotropy Probe results (Komatsu et al. 2009) and was also adopted by S11. The adopted baryon fraction is 0.1658.

In the following we summarise the main aspects of the modelling of the dust attenuation and emission. A more detailed account can be found in S11.

2.1.1 Model for Dust Attenuation

Our model for dust extinction is based on the approach proposed by Guiderdoni & Rocca-Volmerange (1987), combined with the model proposed by Charlot & Fall (2000). As in the Charlot & Fall model, we consider extinction by two components, one due to the diffuse dust in the disc and another associated with the dense 'birth clouds' surrounding young

star forming regions. The V-band, face-on extinction optical depth of the diffuse dust is given by

$$\tau_{V,0} = \frac{\tau_{\text{dust},0}\, Z_{\text{cold}}\, m_{\text{cold}}}{r_{\text{gas}}^2} \quad , \tag{1}$$

where $\tau_{\text{dust},0}$ is a free parameter, Z_{cold} is the metallicity of the cold gas, m_{cold} is the mass of the cold gas in the disc, and r_{gas} is the radius of the cold gas disc, which is assumed to be a fixed multiple of the stellar scale length.

To compute the actual extinction we assign a random inclination to each galaxy and use a standard 'slab' model; i.e. the extinction in the V-band for a galaxy with inclination i is given by:

$$A_V = -2.5 \log_{10} \left[\frac{1 - \exp\left(\frac{-\tau_{V,0}}{\cos(i)} \right)}{\frac{\tau_{V,0}}{\cos(i)}} \right] \quad . \tag{2}$$

Additionally, stars younger than t_{BC} are enshrouded in a cloud of dust with optical depth $\tau_{\text{BC,V}} = \mu_{\text{BC}}\, \tau_{V,0}$, where we treat t_{BC} and μ_{BC} as free parameters. Finally, to extend the extinction estimate to other wavebands, we assume a starburst attenuation curve (Calzetti 1997, 2001) for the diffuse dust component and a power-law extinction curve $A_\lambda \propto (\lambda/5500\text{Å})^n$, with $n = 0.7$, for the birth clouds (Charlot & Fall 2000). Our results are insensitive to minor modifications of the underlying extinction curve for the cirrus extinction, e.g. adoption of a Galactic or SMC-type extinction curve instead of Calzetti.

2.1.2 Dust Parameters

There are three free parameters that control the dust attenuation in our model: the normalization of the face-on V-band optical depth $\tau_{\text{dust},0}$, the opacity of the birth clouds relative to the cirrus component μ_{BC}, and the time that newly born stars spend enshrouded in their birth clouds, t_{BC}. We first set $\tau_{\text{dust},0}$ by matching the normalization of the observed relationship between $L_{\text{dust}}/L_{\text{UV}}$ vs. bolometric luminosity L_{bol} for nearby galaxies, where L_{dust} is the total luminosity absorbed by dust and re-emitted in the mid- to far-IR and L_{UV} is the luminosity in the far-UV (~ 1500 Å). Using a value of $\tau_{\text{dust},0} = 0.2$, S11 found good agreement with these observations, and also with the observed optical through NIR luminosity functions in the local Universe. We also adopt this same value, $\tau_{\text{dust},0} = 0.2$.

The birth cloud parameters μ_{BC} and t_{BC} mainly control the attenuation of UV light relative to longer wavelengths. S11 show that in the local Universe ($z = 0$), the g through K-band luminosity functions are insensitive to the birth cloud parameters, while the FUV through u-bands are quite dependent on them. S11 adjusted the parameters to match the $z = 0$ FUV and NUV observed luminosity functions, finding good agreement with $\mu_{\text{BC}} = 4.9$ and $t_{\text{BC}} = 2 \times 10^7$ yr, which we also adopt in our study. However, S11 found that it was not possible to reproduce the observed rest-UV and optical luminosity functions at high redshift with fixed values of these parameters. Other studies (e.g. Lo Faro et al. 2009; Guo & White 2009) have reached similar conclusions. Moreover, there is direct observational evidence that galaxies are less extinguished at high redshift for a given bolometric luminosity (Reddy et al. 2010). Following S11, we therefore

adopt a simple redshift dependence in all three dust parameters, which is adjusted in order to reproduce the observed rest-frame UV and optical luminosity functions out to $z \sim 5$. Our adopted scalings are: $\tau_{\text{dust},0}(z) = \tau_{\text{dust},0}(1 + z)^{-1}$, and both μ_{BC} and t_{BC} scale with z^{-1} above $z = 1$.

2.1.3 Model for the Dust Emission

Using the formalism presented above we can compute the total fraction of the energy emitted by stars that is absorbed by dust, over all wavelengths, for each galaxy in our simulation. We then assume that all of this absorbed energy is re-radiated in the IR (we neglect scattering), and thereby compute the total IR luminosity of each galaxy L_{IR}. We then make use of dust emission templates to determine the SED of the dust emission, based on the hypothesis that the shape of the dust SED is well-correlated with L_{IR}. The underlying physical notion is that the distribution of dust temperatures is set by the intensity of the local radiation field; thus more luminous or actively star forming galaxies should have a larger proportion of warm dust, as observations (e.g. Sanders & Mirabel 1996) seem to imply.

There are two basic kinds of approaches for constructing these sorts of templates. The first is to use a dust model along with either numerical or analytic solutions to the standard radiative transfer equations to create a library of templates, calibrated by comparison with local prototypes. This approach was pioneered by Desert, Boulanger & Puget (1990), who posited three main sources of dust emission: polycyclic aromatic hydrocarbons (PAHs), very small grains and big grains. In this approach, the detailed size distributions are modelled using free parameters, which are calibrated by requiring the model to fit a set of observational constraints, such as the extinction or attenuation curves, observed IR colours and the IR spectra of local galaxies.

The second approach is to make direct use of observed SEDs for a set of prototype galaxies and to attempt to interpolate between them (e.g. Chary & Elbaz 2001; Dale & Helou 2002; Lagache et al. 2004). In this work we make use of the empirical SED templates recently published by Rieke et al. (2009), hereafter R09. They constructed detailed SEDs from published ISO, IRAS and NICMOS data as well as previously unpublished IRAC, MIPS and IRS observations. They modelled the far infrared SEDs assuming a single blackbody with wavelength-dependent emissivity. The R09 library includes fourteen SEDs covering the $5.6 \times 10^9 L_\odot < L_{\text{IR}} < 10^{13} L_\odot$ range. To explore the sensitivity of our results to the details of the template set, we also present results for the Chary & Elbaz (2001) templates, hereafter CE01, and for the templates recently presented by Chary & Pope (2010), hereafter CP11. The latter are calibrated to reproduce the SEDs of high redshift galaxies, which appear to deviate somewhat from the local templates (for a detailed discussion, see CP11).

2.2 The Mock Light Cone

We use the SAM described in Section 2.1 to generate a mock light cone of simulated galaxies. Our simulated light cone is 100 times the size of the Great Observatories Origins Deep Survey (GOODS) on the northern sky, which covers ~ 160

arcminutes squared in the sky. We chose to simulate a light cone that covers 100 times larger area than the GOODS-N to improve the statistics, as luminous IR galaxies are relatively rare. We further limit our light cone of simulated galaxies to range from zero to six in redshift space. This limitation is arbitrary, however, we will show below that the apparent IR flux of simulated galaxies drops steeply as a function of redshift, so that it is unlikely that any galaxies beyond this redshift could be detected by *Herschel*.

Our simulated light cone contains in total $23,980,599$ galaxies. The dark matter halo masses range from $\sim 2.7 \times 10^9$ to $\sim 4.5 \times 10^{14} \mathrm{M}_\odot$. Consequently, our lightcone contains a variety of dark matter haloes from light subhaloes to large and massive cluster sized haloes. As a result, these simulated dark matter haloes host a variety of different types of galaxies from small dwarf galaxies to giant ellipticals. The stellar masses of our simulated galaxies range roughly five orders in magnitude from 10^7 to $\sim 4.6 \times 10^{12} \mathrm{M}_\odot$.

We use the full mock light cone from redshift zero to six when comparing the predicted number counts to observational constraints (Section 3.1) and for predictions of the galaxy luminosity functions (Section 3.2). We also use all galaxies in our full mock light cone when making predictions for physical properties as a function of redshift. However, in some cases we select a subsample that contains only high-redshift IR bright galaxies.

2.2.1 Sample of High-Redshift luminous IR Galaxies

For part of our analysis, we focus on a sample with criteria that are motivated by the desire to compare with high redshift galaxies in the GOODS-*Herschel* survey. For this sample, we select all simulated galaxies from our light cone that are in the redshift range $2 \leq z < 4$ and above the detection limit of either PACS at the 160 μm or SPIRE at the 250 μm bands in the GOODS North. For simplicity, we assume the limits for both instruments to be ~ 5 mJy (see, e.g. Elbaz et al. 2010), although we note that the actual detection limit in the PACS band may be somewhat lower ($\sim 3.5 - 4.5$ mJy). These two bands were chosen to represent the two different instruments and to be close to the peak of the thermal IR emission in our chosen redshift range. No other selection criteria, such as stellar mass or optical flux cut, were applied, except the ones enforced by the mass resolution.

Selected in this way, our high-redshift sample comprises in total 1154 (3948) galaxies when the selection is done using the PACS 160 (SPIRE 250) μm band. Note however that our simulated light cone is 100 times larger than the GOODS-N — hence one may infer that we would expect ~ 10 PACS 160 μm and ~ 40 SPIRE 250 μm detected galaxies in a field with the size and depth of GOODS-N. However, cosmic variance is probably large for these objects, and therefore this number is uncertain. We return to this matter in the following Sections.

The PACS 160 μm selected high-redshift sample consists of luminous IR galaxies with bolometric IR luminosity ranging from $\sim 1 \times 10^{12}$ to $\sim 2 \times 10^{13} \mathrm{L}_\odot$. The average bolometric luminosity $\bar{L}_{\mathrm{IR}} \sim 2.46 \times 10^{12} \mathrm{L}_\odot$. The SPIRE 250 μm selected high-redshift sample consists of IR bright galaxies with the bolometric IR luminosity ranging from $\sim 5 \times 10^{11}$ to $\sim 2 \times 10^{13} \mathrm{L}_\odot$, while the average bolometric IR luminos-

ity $\bar{L}_{\mathrm{IR}} \sim 1.75 \times 10^{12} \mathrm{L}_\odot$. We can therefore readily conclude that all of the galaxies in the PACS selected sample are ULIRGs, while in the SPIRE selected sample they are at least LIRGs, while most, i.e. more than 90 per cent, can be defined as ULIRGs. The simple single PACS 160 μm or SPIRE 250 μm band selection is a good indicator for the total IR luminosity because in our selected redshift range we are always near the peak of the IR flux. Consequently, our sample of high-redshift galaxies is well suited to study the physical properties of high redshift (U)LIRGs that are potentially observable in fields such as the GOODS North and South.
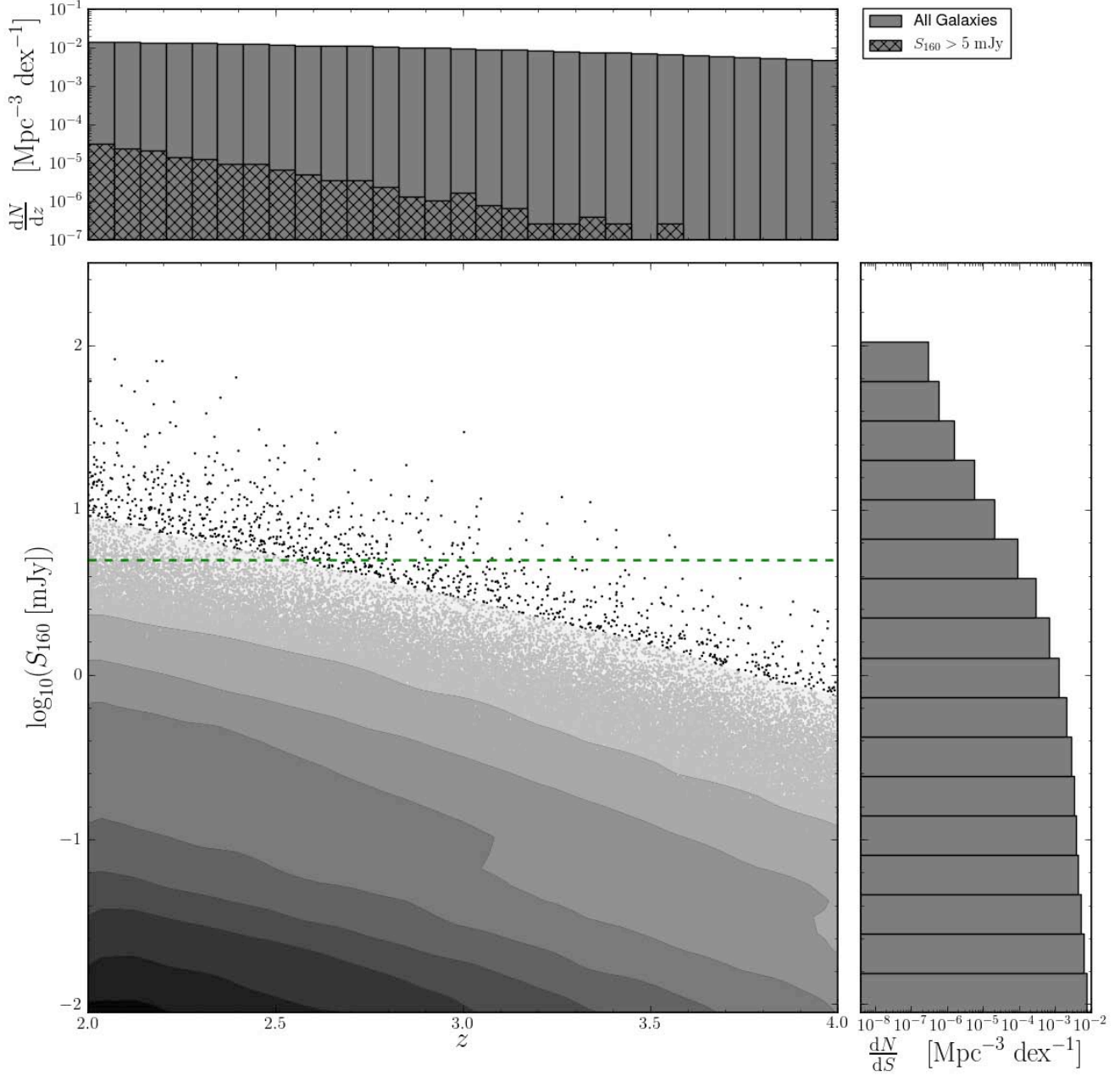
Figure 1 shows the PACS 160 μm flux, S_{160}, in mJy as a function of redshift z for all simulated galaxies as well as the co-moving number density of simulated galaxies as a function of PACS 160 μm flux and redshift. The horizontal green dashed line in the scatter plot is drawn at 5 mJy, which is roughly the same as the detection limit in the GOODS-N. Note, however, that the confusion limit in the GOODS-N and in comparable fields can be higher than the detection limit, especially at longer wavelengths. For example, a confusion limit $\sim 19.1 \pm 0.6$ mJy at the 250 μm SPIRE band has been quoted in literature (Nguyen et al. 2010). Obviously, observations that are of the same depth, but on less crowded fields could reach down to the mJy level. Moreover, observations in gravitational lensed fields can reach well below the derived confusion limit, as has already been shown by Altieri et al. (2010), thus providing a motivation for our sample selection and the usage of 5 mJy. We note that the Fig. 1 would be quantitively similar if we used the SPIRE 250 μm band instead of the PACS 160 μm flux, although the SPIRE-selected sample extends to slightly higher redshift (a few galaxies are predicted above 5 mJy up to $z \sim 4.0$).

Figure 1 shows that the number density of luminous IR galaxies drops quickly above redshift three, hence, observations comparable to those in GOODS-N are unlikely to detect galaxies above redshift four. However, as noted above, these galaxies are likely to be strongly clustered, with a large field-to-field variance, implying that the maximum redshift may also vary from field to field. Unfortunately, due to the fact that we adopt the Extended Press-Schechter formalism to generate our merger trees, we do not have information on the spatial locations of our galaxies and therefore we cannot properly quantify the effects of cosmic variance. We defer this to a future study, where we plan to use lightcones extracted from N-body simulations and will therefore have information on the clustering properties of our galaxies.

3 OBSERVABLE PROPERTIES

3.1 Number Counts and Redshift Distributions

The most basic statistic describing a galaxy population is the number counts, i.e. the number density on the sky of galaxies as a function of observed flux. The number counts at far-infrared and sub-mm wavelengths are well known to exhibit strong evolution (Oliver et al. 2010, and references therein). Unfortunately, the *Herschel* beam is broad compared to the number density of sources, and thus the maps are often confused. This confusion means that care has to be taken when estimating number counts from *Herschel* data:

Figure 1. PACS 160 μm flux, S_{160}, in mJy as a function of redshift z for all simulated galaxies. The histograms show projections of the scatter plot. The solid bars in the upper histogram show co-moving number density ($\frac{\mathrm{d}N}{\mathrm{d}z}$) of all galaxies, while the hatched bars show that of simulated galaxies with $S_{160} > 5$ mJy. The right-hand side histogram shows co-moving number density ($\frac{\mathrm{d}N}{\mathrm{d}S}$) as a function of PACS 160 μm flux. The horizontal green dashed line is at 5 mJy, which corresponds roughly to the detection limit in PACS 160 μm observations in the GOODS-N.

observations must in general be corrected for flux boosting and incompleteness (see, e.g., Clements et al. 2010; Oliver et al. 2010, and references therein). For example, the faint flux densities may be overestimated due to the classical flux boosting effect (e.g. Béthermin et al. 2010). In the following sections we therefore compare our model to existing observations and make predictions for higher redshifts and lower flux levels than what the current observations have probed.

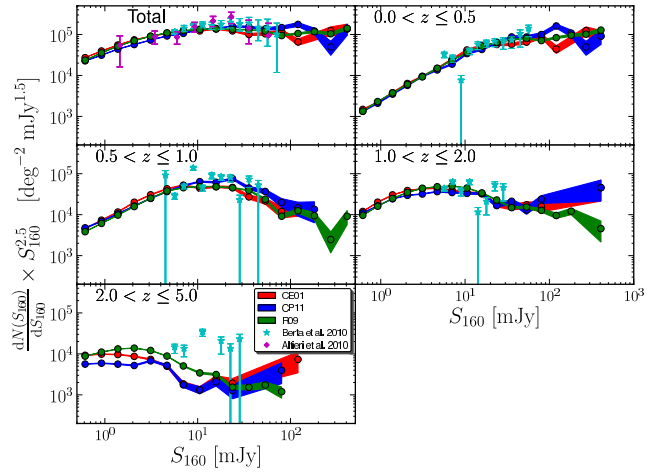### 3.1.1 *Number Counts in the PACS and SPIRE Bands*

Figures 2 and 3 show differential galaxy number counts for the PACS 100 and 160 μm bands derived from our simulated light cone after being normalised to a Euclidean slope ($\mathrm{d}N/\mathrm{d}S \propto S^{-2.5}$). In order to investigate the sensitivity of our results to the dust emission templates, we have shown the predictions using three different sets of templates. The
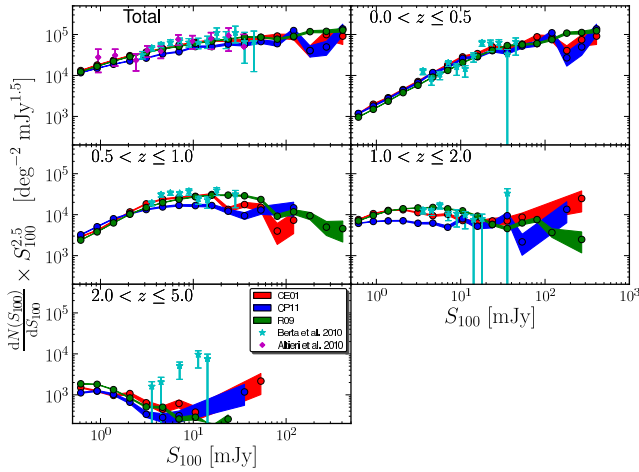
Figure 2. Predicted galaxy differential number counts (circles) compared to observational estimates of Berta et al. (2010) (shown in cyan) and Altieri et al. (2010) (shown in magenta) in the PACS 100 μm band at different redshift bins. The Berta et al. (2010) observations are based on direct detections, while the Altieri et al. (2010) number counts take advantage of lensing caused by the cluster Abell 2218. The shaded regions correspond to 3σ Poisson errors in the model, while the observational errors are 1σ limits. The different colours refer to different dust emission template SEDs that have been used in the semi-analytic model (red: Chary & Elbaz (2001); blue: Chary & Pope (2010); green: Rieke et al. (2009)).
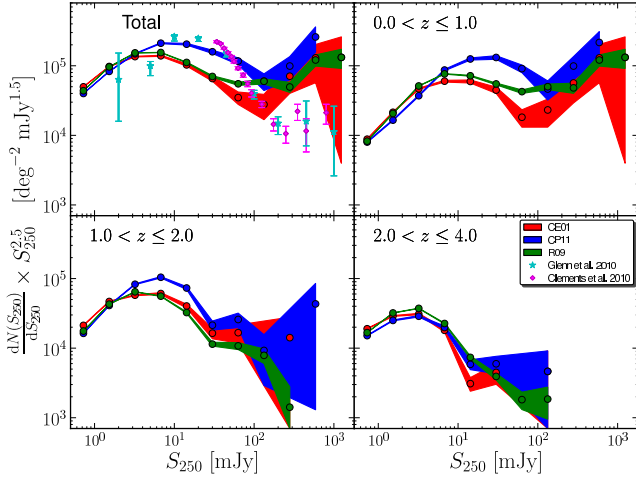
Figure 3. Predicted galaxy differential number counts (circles) compared to observational estimates of Berta et al. (2010) (shown in cyan) and Altieri et al. (2010) (shown in magenta) in the PACS 160 μm band at different redshift bins. The Berta et al. (2010) observations are based on direct detections, while Altieri et al. (2010) number counts take advantage of lensing caused by Abell 2218. The shaded region corresponds to 3σ Poisson errors in the model, while the observational errors are 1σ limits. The different colours refer to different dust emission template SEDs that have been used in the semi-analytic model (red: Chary & Elbaz (2001); blue: Chary & Pope (2010); green: Rieke et al. (2009)).

template sets of Rieke et al. (2009) and Chary & Elbaz (2001) are based on nearby galaxies. The templates of Chary & Pope (2010) incorporate data from distant galaxies, and in general predict higher fluxes longwards of the thermal dust peak for IR luminous galaxies, corresponding to colder dust temperatures. Overplotted are the galaxy differential number counts from the early *Herschel* observations of Berta et al. (2010) and Altieri et al. (2010). The number counts of Berta et al. (2010), which were derived from GOODS-N data, cover the flux range $3 - 50$ mJy at 100 μm and $5.5 - 72$ mJy at 160 μm, while the number counts of Altieri et al. (2010) cover the flux range $\sim 1 - 35$ and $\sim 1.5 - 58$ mJy at 100 and 160 μm, respectively. The general agreement between the galaxy differential number counts of simulated galaxies and observations is excellent at low ($z < 2$) redshift. However, in the highest redshift bin ($2 < z \leq 5$) the agreement is worse. Even though the observational constraints are weaker — only two (four) of the observational constraints at the PACS 100 (160) μm band are not upper limits — this disagreement requires further discussion. We return to this issue later.

A detailed inspection of the differential number counts of the simulated galaxies shows a monotonic rise in the two lowest redshift bins till ~ 20 mJy. This is consistent with a non-evolving population of galaxies. Based on their observations Berta et al. (2010) argue for a drop at ~ 20 mJy, even though the errors in observations are relatively large. The number counts of the simulated galaxies provide some support for such a claim at the 100 μm band, however, at the 160 μm band our model does not show any significant drop. For the PACS 100 μm band our model predicts a reasonably monotonic rise all the way to ~ 500 mJy. Even so, a small

(but statistically significant) drop is visible at ~ 60 mJy. Quantitatively the PACS 160 μm band's behaviour is very similar, however, the increase in the Euclidean normalised number counts is shallower after ~ 20 mJy and seems to reach a plateau. The Euclidean normalised counts seem to rise again at ~ 200 mJy, especially at the PACS 100 μm band.

The redshift evolution of the galaxy differential number counts of the simulated galaxies in both PACS 100 and 160 μm bands is rather modest at $z \lesssim 1$. Even up to redshift two the number of ~ 10 mJy IR galaxies seems to evolve only slowly, in contrast to the number of fainter galaxies, which seems to grow as a function of redshift, causing the distribution of the number counts to flatten and eventually to turn over when probing even earlier cosmic times. At $z \gtrsim 2$ our model predicts that the normalised number counts of the faintest ($S_{160} \sim 0.1$ mJy) galaxies are at the same level as that of the brightest ($S_{160} \sim 100$ mJy).

Figures 4, 5, and 6 show Euclidean normalised differential galaxy number counts derived from our simulated light cone in the 250, 350, and 500 μm SPIRE bands, respectively. We show the observational results from the early *Herschel* observations of Glenn et al. (2010) and Clements et al. (2010) for comparison. At 250 μm, our model predicts significantly fewer galaxies at the $5 - 30$ mJy level than are observed. This discrepancy is even larger in the SPIRE 350 and 500 μm bands. The agreement seems better at slightly higher fluxes (~ 100 mJy), but then the models overpredict sources at the highest flux levels (~ 1 Jy) in all three bands. Note however that the number of simulated galaxies with $S \gtrsim 400$ mJy is very small, as indicated by the large errorbars. The actual field-to-field variation will be even larger, as
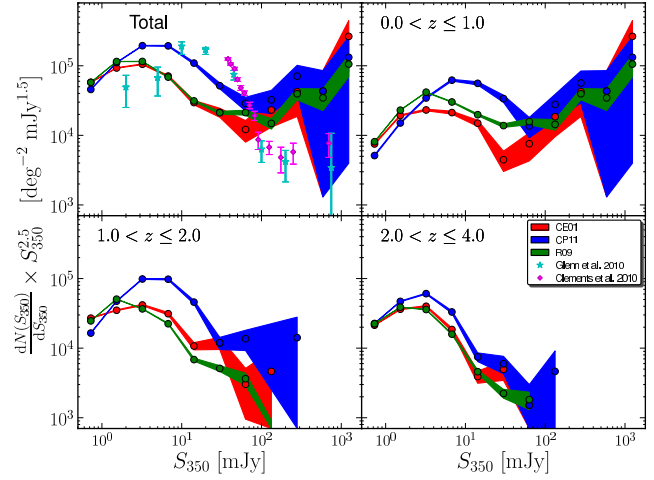
Figure 4. Predicted galaxy differential number counts (circles) compared to observational estimates of Glenn et al. (2010) (shown in cyan) and Clements et al. (2010) (shown in magenta) in the SPIRE 250 μm band in different redshift bins. The number counts of Clements et al. (2010) are direct detections, while Glenn et al. (2010) derived their counts by modelling the $P(D)$ distribution, rather than identifying individual galaxies. The shaded regions correspond to 3σ Poisson errors in the models, while the observational errors are 1σ limits. Green, red, and blue colours show the predictions using different dust emission templates, as in the previous figures.

Figure 5. Predicted galaxy differential number counts (circles) compared to observational estimates of Glenn et al. (2010) (shown in cyan) and Clements et al. (2010) (shown in magenta) in the SPIRE 350 μm band at different redshift bins. The number counts of Clements et al. (2010) are direct detections, while Glenn et al. (2010) derived their counts by modelling the $P(D)$ distribution, rather than identifying individual galaxies. The shaded regions corresponds to 3σ Poisson errors in the models, while the observational errors are 1σ limits. Green, red, and blue colours show the predictions using different dust emission templates, as in the previous figures.
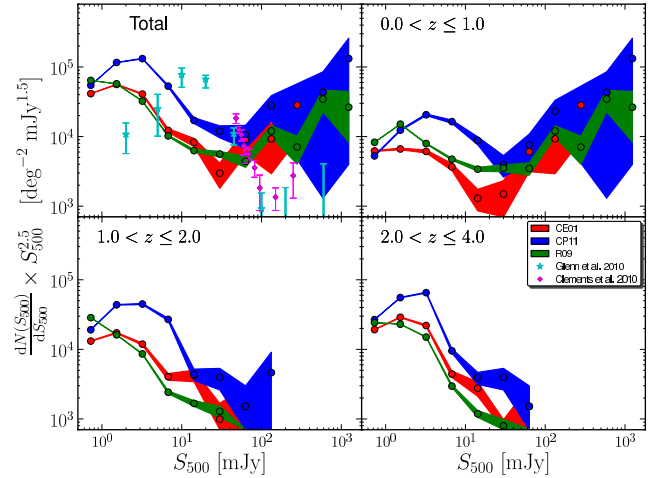
our model errorbars do not include the effects of large-scale clustering.

The galaxy differential number count estimates of Glenn et al. (2010) are based on the pixel brightness distribution $P(D)$ method, in which no direct detections are needed. In this method the distribution of pixel brightnesses are used to make statistical interferences about the slope and amplitude of the source counts. Therefore, the $P(D)$ method can be used to derive number counts below the confusion limit (see Glenn et al. (2010) for details). However, we note that Glenn et al. (2010) emphasise that their values are *model fits* and thus effectively integral constraints over some region surrounding each flux density. However, as the differences between their multiply-broken power-law and spline models are relatively small, we choose to show only their results based on the multiply-broken power-law model (Table 2 of Glenn et al. 2010). This provides a reasonable compromise given the fact that we have added their 1σ statistical errors and their estimated systematic uncertainties in quadrature, after which both of their model fits are roughly within the errors shown.

Glenn et al. (2010) note that they clearly detect a break in the number counts at around 20 mJy in all the SPIRE bands at high significance. Our model also shows a break, however, it is at a significantly lower flux ($\sim$ 2 mJy), except for the SPIRE 250 μm channel when adopting the Chary & Pope (2010) templates. Glenn et al. (2010) also note that there is possible weak ($\sim 1\sigma$) evidence for a 'bump' in the differential counts around 400 mJy at the 250 μm band. The location of such a bump in our models is quite dependent on the adopted dust emission templates, but our model shows an upturn at high fluxes independent of the templates adopted. However, at the 350 μm band all templates show a

Figure 6. Predicted galaxy differential number counts (black circles) compared to observational estimates of Glenn et al. (2010) (shown in cyan) and Clements et al. (2010) (shown in magenta) in the SPIRE 500 μm band at different redshift bins. The number counts of Clements et al. (2010) are direct detections, while Glenn et al. (2010) derived their counts by modelling the $P(D)$ distribution, rather than identifying individual galaxies. The shaded regions correspond to 3σ Poisson errors in the models, while the observational errors are 1σ limits. Green, red, and blue colours show the predictions using different dust emission templates, as in the previous figures.

bump around 300 mJy, although it is unclear whether this is part of the upturn or a real feature given the relatively large uncertainties at high fluxes.

We are not aware of any published results for SPIRE counts broken into redshift bins, however we show our theoretical predictions for comparison with future observational results. The predicted redshift evolution of the number counts in all SPIRE bands is qualitatively similar to that of the PACS bands. We note however that in the SPIRE bands the redshift evolution of LIRGs is more modest. Even in the highest redshift bin, the Euclidean normalised galaxy differential number counts of the brightest galaxies are only a factor of a few lower than in the lower redshift bins.

In summary, our models produce very good agreement for the overall counts in the PACS 100 and 160 μm bands, but this agreement rapidly worsens as we move to longer wavelengths. The overall agreement in the SPIRE bands is quite poor. Moreover, although our model predictions are also in good agreement with the galaxy number counts split by redshift for $z < 2$, they do not produce enough IR-luminous galaxies at $z > 2$. Although the magnitude of the discrepancy between our theoretical predictions and the observational results is disturbing, the interpretation is also somewhat complex. In what follows we therefore discuss potential theoretical and observational complications that could lead to the noted discrepancies in turn.

We first emphasise that these semi-analytic models have been shown elsewhere (see S11; Fontanot et al. 2009a, and references therein) to reproduce reasonably well observed luminosity functions from the rest UV to near-IR, as well as stellar mass functions and star formation rate functions, from $z \sim 0 - 5$, although the agreement does get worse towards higher redshifts. Moreover, the good agreement in the PACS bands up to $z \sim 2$ suggests that many of the basic ingredients of the model must be reasonable. However, a possible explanation for some of these discrepancies is that perhaps the adopted dust emission templates are not valid at earlier cosmic times. Indeed, there is observational evidence that the correlation between total IR luminosity and dust temperature might be different in high redshift galaxies (Amblard et al. 2010; Elbaz et al. 2010; Hwang et al. 2010). We attempted to investigate this by testing three different sets of dust emission templates (see also the discussion in CP11), as described at the beginning of this section. The results of adopting the different templates are complex, with some templates producing better results at some wavelengths and redshifts, and others performing better in other regimes. The predictions with the three templates are similar in the PACS bands for the overall counts and at low redshifts ($z < 1$). The CP11 templates predict slightly fewer galaxies in the highest redshift bin ($2 < z < 5$), which worsens the (already poor) agreement with the observations. However, the CP11 templates produce significantly better agreement for the counts in the SPIRE bands at intermediate fluxes (between about 3 and 100 mJy). Thus, we conclude that the results are sensitive to the choice of dust emission templates, but none of the template sets that we investigated can reproduce the observations at all wavelengths. Another potential cause for the noted discrepancy may relate to our simplified modeling of the dust absorption and emission. We tuned our model to reproduce the observed ratio of unattenuated to re-radiated light (UV to FIR) for *average* galaxies at $z = 0$.

However, galaxies at high redshift may have more complex geometries, leading to greater scatter or even a breakdown in this approach. As already noted, scatter or evolution in the dust emission SEDs could also be important. As noted by CP11, it is not clear whether the observations they used span the entire range of underlying dust temperatures and associated far-infrared colours.

On the other hand, one likely culprit in the *Herschel* observations is the impact of flux boosting and blending, which affects the counts more severely at longer wavelengths and may also have a larger effect at high redshifts, where galaxies are strongly clustered and there is a higher probability that the *Herschel* beam intersects lower redshift objects along the line of sight. Indeed, we have visually checked the Hubble Space Telescope (HST) images at the position of 250 μm detected *Herschel* sources in GOODS-N, and it is clear that in many, if not most cases, there are multiple galaxies within the PACS or SPIRE beam. For longer wavelengths such as the SPIRE 500 μm the complications are even worse because of the full-width-at-half maximum of the beam doubles (from ~ 18 at 250 μm to ~ 36 arc seconds). Moreover, according to the simulations carried out by Rigby et al. (2011), more than half (~ 57 per cent) of sources detected at $\geq 5\sigma$ at 500 μm show a flux boosting by a factor > 1.5 and more than every fourth (~ 27 per cent) by a factor > 2. This is clearly a very serious issue when comparing theoretical predictions with these observations.

Other observational complications include cosmic variance. Particularly the bright counts may be compromised by field-to-field variance, as the areas covered are still not large. Moreover, at long wavelengths, recent results imply that many of the bright sources might be lensed (e.g. Negrello et al. 2010; Lima, Jain & Devlin 2010; Lima et al. 2010). Finally, the contribution to the dust heating from obscured active galactic nuclei (AGN) is uncertain (e.g. Almaini, Lawrence & Boyle 1999; Granato, Danese & Franceschini 1997; Farrah et al. 2007; Sajina et al. 2008), although this is unlikely to contribute significantly particularly at the longer wavelengths. Because we cannot rule out these effects, for the remainder of this work, we therefore caution that the predicted IR fluxes that we quote should not be interpreted as corresponding in a one-to-one fashion with the measured fluxes for individual sources that can currently be detected in a *Herschel* image, but rather with the idealised flux that one would obtain if flux boosting, blending, and cosmic variance could be overcome. This situation is less than ideal, but we feel that it can provide a first step towards providing useful predictions. In future work, we plan to pursue a more rigorous comparison, in which we use the theoretical simulations to produce mock *Herschel* images and treat them in the same way as the real observations. Moreover, the GOODS-*Herschel* team and others are also working on a better understanding of the impact of blending on their observations, which will eventually clarify the interpretation of our predictions. In addition, our predictions in this form can be compared directly with other theoretical predictions in the literature, which similarly do not address the effects of blending.

3.2 Galaxy Luminosity Functions

While simple number counts are the most basic statistic of galaxy populations, their predictive power is limited. A step further towards the intrinsic properties of a galaxy population can be taken by studying the galaxy luminosity functions (LFs). However, even more knowledge of galaxy evolution can be gathered when the evolution of the rest-frame LFs are studied as a function of redshift.

Figure 7 shows the rest-frame galaxy LFs in the PACS 100 and 160 μm and SPIRE 250 and 350 μm bands. The rest-frame galaxy LFs are shown in five different redshift bins: $0 \leq z < 0.3$, $1.2 \leq z < 1.6$, $2.0 \leq z < 2.4$, $2.4 \leq z < 4.0$, and $4.8 \leq z < 5.1$. This enables the study of the redshift evolution of the galaxy IR LFs between $z \sim 5$ and $z \sim 0$. Unfortunately the observational constraints in the rest-frame LFs of *Herschel* bands are still limited, especially at higher redshifts, thus, the comparison between the theoretical predictions and observations is less than robust. However, to provide an initial comparison we show the LFs of Lapi et al. (2011), which have been derived from early *Herschel* data. The redshift bins of the theoretical LFs have been matched to the ones presented in Lapi et al. (2011) to allow easy comparison. However, the sample of Lapi et al. (2011) is limited to only bright galaxies with $S_{250} \geq 35$ mJy. Moreover, even though they estimate that the fraction of false identifications is as low as ~ 6 per cent (in areas with good SDSS completeness), they warn that some truly high-z sources can be missed by their study leading to incompleteness as high as 20 per cent. Such complications will obviously make the comparison less than robust.

The upper panels of Figure 7, namely a and b, show the predicted galaxy LFs in the PACS 100 and 160 μm bands. Qualitatively these two panels are rather similar, i.e., there are only small differences in the LFs of the rest-frame 100 and 160 μm bands. We do note however that the 160 μm band does not extend to as high luminosities as the 100 μm band. This is true at all redshifts. The rest-frame LF of the lowest redshift bin is the lowest curve, showing that the redshift evolution in the PACS bands is strong. The two panels show that the number density of the PACS bright galaxies is highest at redshifts $z \sim 2$, while the highest number density of the faint galaxies is found at $z \sim 3$. Both PACS bands show that the faint end of the LFs evolves hardly at all between $z \sim 5$ and $z \sim 2$. Even though we do not see much evolution in the faint end of the PACS LFs, a clear difference exists between the local and higher redshift galaxies. Our model predicts that the number density of luminous infrared galaxies peaks around $z \sim 2 - 3$, in agreement with other predictions (e.g. Swinbank et al. 2008; Lacey et al. 2010). Furthermore, the total number of IR bright galaxies is highest at $z \sim 2$. Such results are easy to understand if the IR rest-frame flux correlates with dust obscured star formation rate, as the cosmic star formation rate density is known to peak around the same cosmic time (e.g. Bouwens et al. 2011). Our model also predicts that the number density of the most luminous IR galaxies (i.e. ULIRGs) increases by a factor of ~ 5 between redshifts five and three, while their number density is found to peak at $z \sim 2$. The evolution of the PACS LFs also shows that the number density of luminous IR galaxies drops by a factor of ~ 10 between redshifts two and zero. These results emphasise the strong evolution

in the number density of (U)LIRGs as a function of cosmic time.

In panel a of Figure 7 we also compare our theoretical LFs to the LFs of Lapi et al. (2011). Qualitatively similar redshift evolution is seen in both cases. Our prediction for the lowest redshift observed LF ($1.2 \leq z < 1.6$) is in reasonable argeement with the observations, with a modest over-prediction of the highest luminosity sources. Towards higher redshift, and especially in the highest redshift bin, the disagreement grows rather large in sense that our model predicts fewer galaxies with high luminosities than are reported in the observations. Similar effects as discussed in the case of number counts are likely to contribute. The most striking difference, however, between our model and the LFs of Lapi et al. (2011) is the location of the knee of the LFs. Our predicted LFs turn over at about two orders of magnitude higher number densities. One potential explanations is provided by Lapi et al. (2011) who argue that the flattening of their LFs at the lowest luminosities may be, at least in part, due to the overestimate of the accessible volume yielded by the $1/V_{\max}$ estimator for objects near to the flux limit.

The lower panels of Figure 7, namely c and d, show the predicted rest-frame galaxy LFs in the SPIRE 250 and 350 μm bands. The redshift evolution of the rest-frame SPIRE band LFs is similar to that of the PACS bands. Again, the number densities of LIRGs and ULIRGs, i.e., the galaxies at the bright end of the LF, are found to peak at $z \sim 2 - 3$. In agreement with the PACS bands, the highest number densities are found at redshifts two and three, while the number densities drop by a factor of ~ 11 to redshift zero. Thus, the LFs of the rest-frame SPIRE bands show qualitatively similar evolution as the LFs of the PACS bands. However, we note that the bright end of the LFs in the SPIRE bands appears to drop more steeply than in the PACS bands.

In panel c of Figure 7 we also compare our theoretical LFs to LFs of Lapi et al. (2011). As in case of the PACS 100 μm the faint end of the lowest redshift LFs ($1.2 \leq z < 1.6$) is in good argeement with our prediction, while in the brightest end our model predicts more galaxies than are observed. Towards higher redshift, and especially in case of the highest redshift bin, the disagreement grows rather large. Again, similar effects as discussed earlier are likely to play a role.

Infrared LFs have also been derived from other observations (e.g. Kim & Sanders 1998; Floc'h et al. 2005; Goto et al. 2010) and early *Herschel* data. Dye et al. (2010) derived SPIRE 250 μm band LFs out to $z = 0.5$. They find that the LF exhibits significant evolution out to $z = 0.5$ and that at a given luminosity, the comoving space density increases steadily with redshift. The evolution noted in Dye et al. (2010) is qualitatively in agreement with our LFs (see S11), although, their evolution is rather strong given the rather narrow redshift range. However, strong evolution, particularly at the bright end, is in agreement with our LFs and also noted by others (e.g. Eales et al. 2009). Also Vaccari et al. (2010) derived LFs for local galaxies in all three SPIRE channels. Their LFs are also in good qualitative agreement with our findings for local galaxies. However, our lightcones have very small volumes at low redshift, as they were intended for high redshift comparisons, so a more quantitative comparison is beyond the scope of this study. A comparison with the $z = 0.5$ SPIRE 250 μm LF is shown in S11.
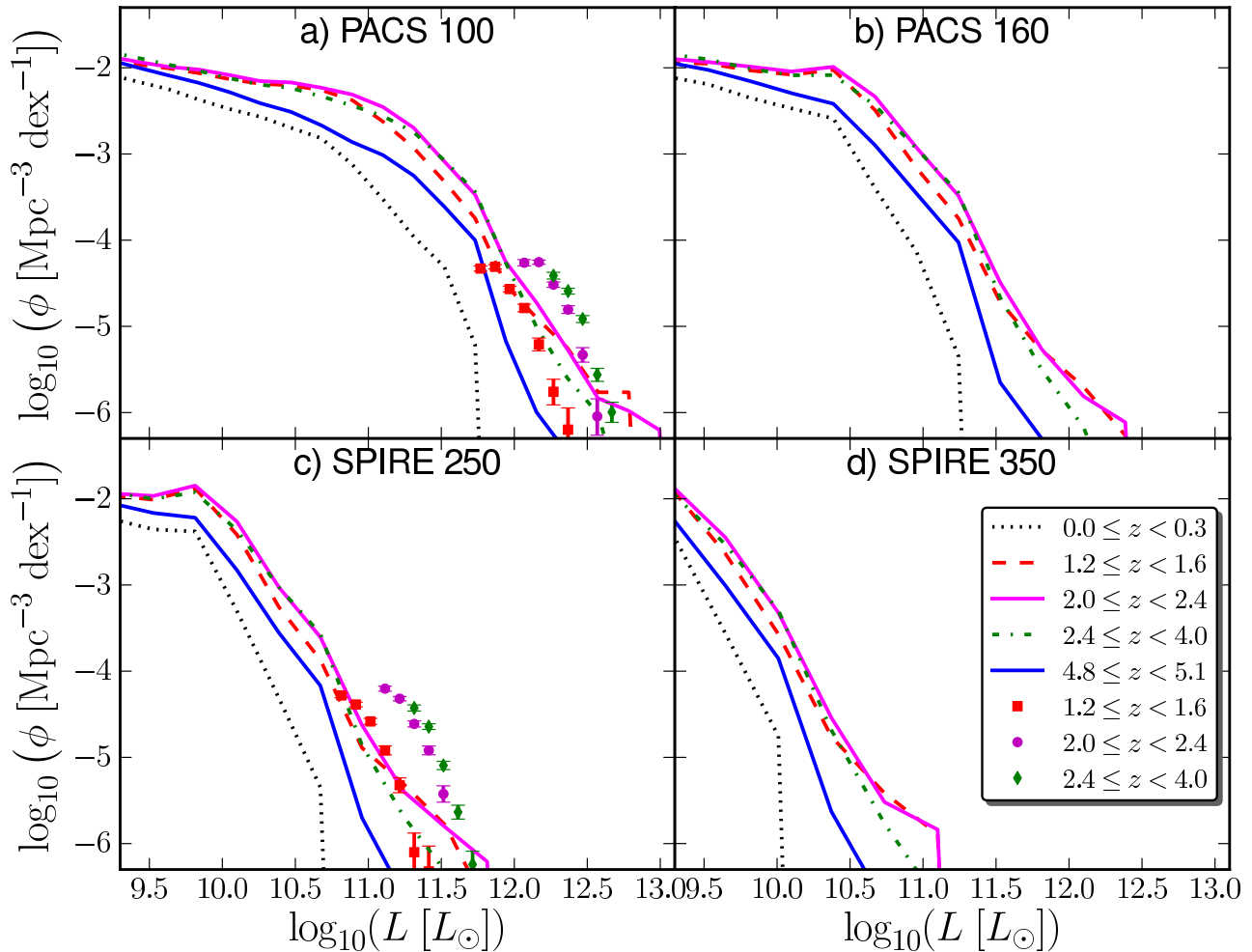
Figure 7. Rest-frame galaxy luminosity functions in the PACS 100 and 160 μm bands and SPIRE 250 and 350 μm bands at five different redshifts. Different redshifts are shown in different colours and are noted in the legend. The observed luminosity functions (in a and c) marked with symbols are from Lapi et al. (2011).

4 PHYSICAL PROPERTIES OF IR-LUMINOUS GALAXIES OVER COSMIC TIME

Having explored some of the statistical properties of *Herschel* detected galaxies, in this Section we present predictions for some of the physical properties of these objects at different redshifts. We explore the correlations between 160 and 250 μm flux and many different physical properties of our model galaxies. Here we show some of the strongest and most interesting correlations that we identified, which include stellar mass, dark matter halo mass, cold gas mass, star formation rate, and total IR or bolometric luminosity. The correlations with the other *Herschel* bands are similar and all qualitative conclusions would remain the same, so we do not show them.

Figure 8 shows the predicted median stellar mass as a function of 160 and 250 μm flux, along with the 16th and 84th percentiles, for different redshifts. Our model predicts that all galaxies with $S_{160} > 5$ or $S_{250} > 5$ mJy have stellar masses in the range $M_\star \sim 10^9 - 10^{11}$ M$_\odot$. Furthermore, we predict that high redshift ($z > 2$) galaxies that can be detected individually in deep *Herschel* surveys such as the GOODS are quite massive, $M_\star \gtrsim 10^{10.5}M_\odot$. This is quite

different from the results of Lacey et al. (2010), who predict much smaller stellar masses for galaxies at a given FIR flux — at $z \gtrsim 2$, even their most luminous galaxies are less massive than $M_\star \sim 10^{10}$M$_\odot$. This difference probably arises mainly from the fact that Lacey et al. (2010) adopted a top-heavy IMF during starbursts. Therefore there are fewer long-lived low mass stars in galaxies at high redshift.

Not surprisingly, as stellar mass is know to be fairly well correlated with dark matter halo mass, we find similar results for the dark matter halo masses. At the lowest redshifts ($z < 0.5$), luminous IR galaxies (with S_{160} or $S_{250} > 5$ mJy) can be found in dark matter haloes as light as $\log_{10}(M_{\rm dm}/M_\odot) \sim 11.1$ (see Fig. 9). However, the bulk of simulated IR bright galaxies with S_{160} or $S_{250} > 5$ mJy, especially at higher redshifts, were found to reside in relatively massive dark matter haloes. To be more precise, our model predicts that the masses of the dark matter haloes of IR bright galaxies can cover a broad range from $\log_{10}(M_{\rm dm}/M_\odot) \sim 11.5$ to 13.5, while the bulk of luminous IR galaxies can be found to reside in rather typical dark matter haloes with masses $\log_{10}(M_{\rm dm}/M_\odot) \sim 12.5$.

These predictions are in good agreement with the re-

cent results of Amblard et al. (2011), which were derived from *Herschel* data. In this paper the authors find an excess clustering over the linear prediction at arcminute angular scales in the power spectrum of brightness fluctuations at 250, 350, and 500 μm. From this excess Amblard et al. (2011) infer that IR bright galaxies are located in dark matter halos with a minimum mass of $\log_{10}(M_{\min}/M_\odot) = 11.5^{+0.7}_{-0.2}$ at 350 μm. When the authors average over the three wavelengths the minimum halo mass for their galaxies is at the level of $3 \times 10^{11} M_\odot$. All our IR bright galaxies are found to reside in dark matter haloes more massive than this lower limit, except a handful of local galaxies, which reside in haloes only slightly less massive ($1 \times 10^{11} M_\odot$) than the minimum mass of Amblard et al. (2011).

Our simulated galaxies show evidence for a weak correlation between the dark matter halo mass and the PACS 160 and SPIRE 250 μm fluxes (Fig. 9). Statistically, galaxies residing in more massive dark matter haloes have higher median IR flux as was also the case with stellar mass (Fig. 8). However, the trend between the dark matter halo mass and 160 or 250 μm flux is weaker than in case of stellar mass as indicated by the larger range between the 16th and 84th percentiles in Fig 9. Moreover, for the high redshift galaxies ($2 \leq z < 4$) with either S_{160} or $S_{250} > 5$ mJy no statistically significant correlation can be inferred. Instead, galaxies with the highest fluxes are again found to reside in dark matter haloes with a broad range of masses from $\log_{10}(M_{\rm dm}/M_\odot) \sim 12$ to 13.5. It is however interesting to note that luminous IR galaxies can also be found in cluster-mass dark matter haloes. This implies that some luminous IR galaxies at high redshift may be the progenitors of present-day brightest cluster galaxies (BCGs). Moreover, this also implies that the IR bright galaxies at high redshifts may provide a signpost to identify proto-clusters during the epoch of their formation. Note, however, that according to our model, the PACS 160 and SPIRE 250 μm fluxes are almost independent of the dark matter halo mass for high-redshift galaxies that would be detected in *Herschel* observations comparable to fields such as the GOODS. Consequently, the IR flux at high redshift must be governed primarily by other quantities than the mass of the dark matter halo.

Figure 10 shows the predicted median mass in cold gas as a function of the PACS 160 and SPIRE 250 μm flux for galaxies selected at different redshifts. Not surprisingly, our model predicts that at high redshift the luminous IR galaxies directly detectable in *Herschel* surveys will be the most gas rich. Our simulation shows that the galaxies found in these surveys should typically be gas rich with cold gas masses ranging from $\sim 10^9$ up to $\sim 4 \times 10^{11} M_\odot$. The bulk of the high redshift IR bright galaxies were found to contain a cold gas mass of $\sim 6 \times 10^{10} M_\odot$. Interestingly, as we noted earlier, the bulk of the high redshift IR bright galaxies have stellar masses $M_\star \sim 6 \times 10^{10} M_\odot$. Consequently, the high-redshift luminous IR galaxies should be extremely gas rich, with the mass in cold gas comparable to or even higher than the mass in stars for high-redshift luminous IR galaxies. This is a clear prediction for future observatories such as ALMA, which should be able to detect CO emission from the molecular gas in these galaxies.

Figure 11 shows the predicted median star formation rate as a function of the PACS 160 and SPIRE 250 μm

flux at different redshifts. It is not surprising that this is the strongest correlation seen so far, as the far-IR flux is generally assumed to be a good proxy for the star formation rate, and at some level this correlation is artificially tight because of our assumed one-to-one correspondence between total IR luminosity (light reprocessed by dust) and dust emission SED. However, this plot provides a convenient guide to what SFR one expects to be able to power galaxies at a given 160 or 250 μm flux at different redshifts, assuming a standard set of templates, as well as an indication of how much scatter can arise from heating of dust by old stars.

Figure 11 shows that at $z > 2$ the galaxies directly detectable in surveys such as the GOODS-N should have median star formation rates $> 30 M_\odot \rm yr^{-1}$ according to our model prediction. We find that the average star formation rate for luminous IR galaxies at a high redshift ($2 \leq z < 4$) is $\sim 155 M_\odot \rm yr^{-1}$. This is significantly higher than for all galaxies (with $\log_{10}(M_{\rm dm}) > 9$) in the same redshift range, for which our model predicts a mean star formation rate of merely $\sim 2 M_\odot \rm yr^{-1}$. The highest star formation rate predicted by our model for a high-redshift galaxy is as high as $\sim 7800 M_\odot \rm yr^{-1}$. In the next Section, we explore the physical mechanisms that are driving high SFRs in high redshift galaxies. Clearly, such high SFR cannot persist for very long periods of time!

Figure 12 shows the median values for the total IR luminosity ($L_{\rm dust}$) as a function of flux in the PACS 160 and SPIRE 250 μm bands at different redshifts. This plot illustrates that, at low redshift, only a very few of the brightest galaxies in our (relatively small volume) simulations would not even be considered LIRGs ($L_{\rm IR} > 10^{11} L_\odot$). Our simulations do not contain any ULIRGs ($L_{\rm IR} > 10^{12} L_\odot$) at low redshift. At $z > 1$, all galaxies above our nominal GOODS-*Herschel* detection limit would be considered LIRGs or ULIRGs, at $z \sim 2$ all of these galaxies would qualify as very bright LIRGs or ULIRGs, and at $z > 3$ all of these galaxies are ULIRGs.

At high redshift ($2 \leq z < 4$) our model predicts median SFRs that are a factor of two higher than those reported in Lacey et al. (2010), as show in Fig. 11. As already noted, Lacey et al. (2010) assumed a top-heavy IMF in starbursts. With a top-heavy IMF, in a given star formation episode, a larger fraction of the mass goes into massive stars that can efficiently heat the dust. Thus, for a top-heavy IMF, the relationship between SFR and IR luminosity is shifted such that a given SFR results in higher IR luminosities. In the Lacey et al. (2010) model, the fraction of star formation occurring in the burst mode increases with redshift, so the average IMF with which stars are being formed shifts from being close to a solar neighbourhood IMF at the present day to being very top-heavy at high redshift. This helps to explain why our SFR vs 250 μm flux relationship agrees with that of Lacey et al. (2010) in the local Universe ($z < 0.25$), but differs significantly at earlier cosmic epochs. In addition, the treatment of dust is also different in the Lacey et al. (2010) model. They used results from the RT+dust model calculations of Silva et al. (1998).
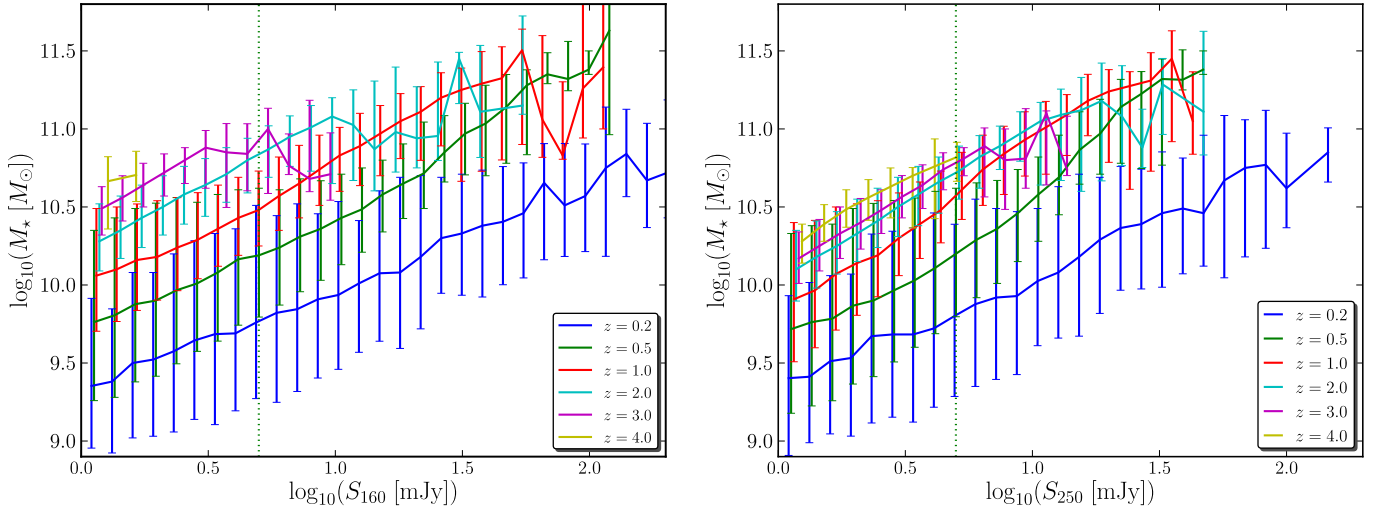
Figure 8. Predicted median stellar mass vs. flux in the PACS 160 and SPIRE 250 μm bands for galaxies selected at different redshifts. The green dotted vertical line shows a representative flux limit of the GOODS-N observations. The error bars show the 16th and 84th percentiles.
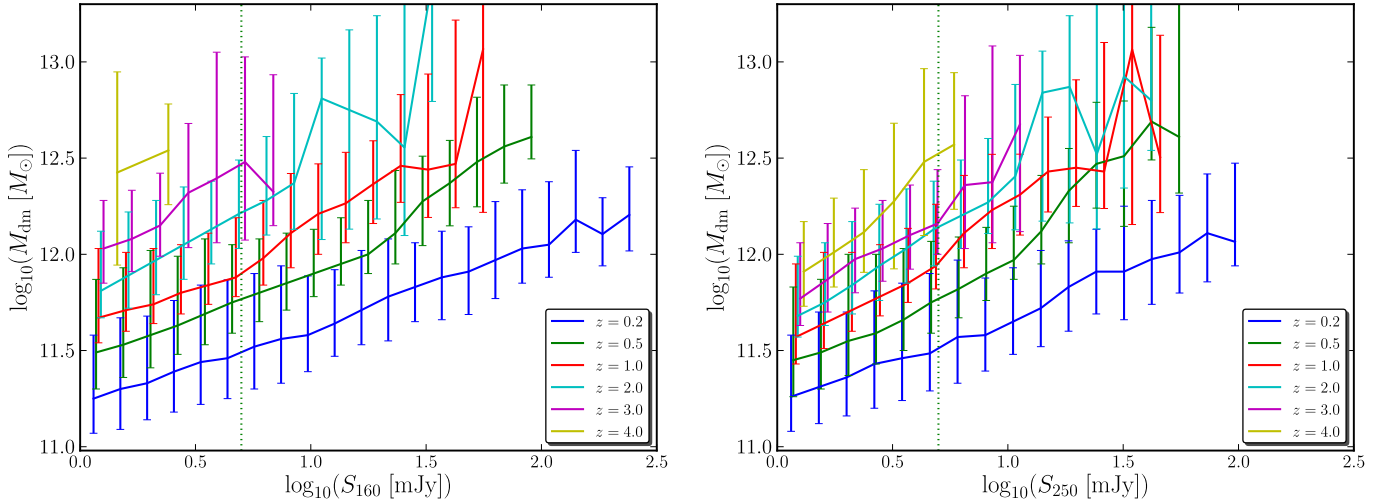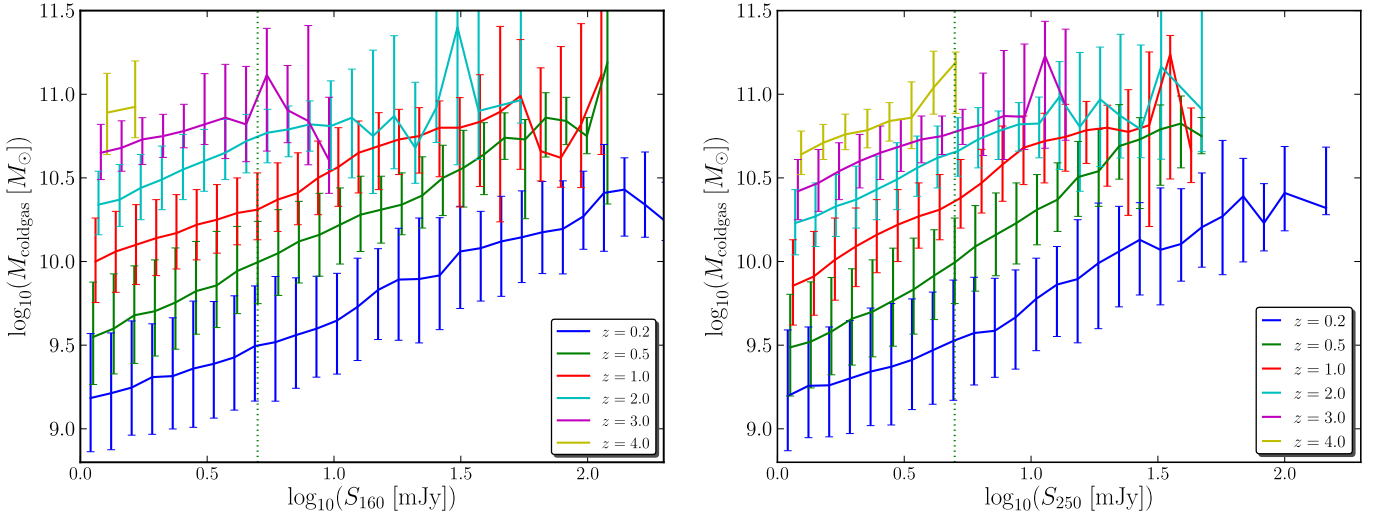

Figure 9. Predicted median dark matter halo mass ($M_{\rm dm}$) as a function of IR flux in the PACS 160 and SPIRE 250 μm bands at different redshifts. The green dotted vertical line shows a representative flux limit for the GOODS-N observations. The error bars show the 16th and 84th percentiles.

4.1 Sizes of High-redshift Late-type Galaxies

For this sub-section we use our "high-redshift" SPIRE 250 μm selected sample of galaxies selected from our light-cones in the redshift range $2 \leq z < 4$. We identify disk galaxies using the bulge to stellar mass ratio: galaxies with $M_{\rm bulge}/M_{\rm total} \leq 0.4$ are considered as late-type galaxies. We also removed all galaxies that have experienced one or more mergers within the last 500 Myr, because these galaxies have disturbed disks (and morphologies) and thus the size of the stellar disk is ill-defined. Figure 13 shows a Hess plot of the galaxy's disk size as a function of its stellar mass $M_\star$ in physical units for this sample of high-redshift galaxies. For a comparison, we also plot the sizes and stellar masses from Cava et al. (2010) with green squares. The gray shading in both panels of Fig. 13 describes the number of simulated galaxies in a given two dimensional bin, while the red lines show the median and 16 and 84 percentiles.

As in the real Universe, our model disks show a positive correlation between stellar mass and radial size. Very few galaxies are predicted to be as large in radial extent as the galaxies presented in Cava et al. (2010). However, the right panel of Figure 13 shows that when we select galaxies in the same redshift range with $S_{250} > 5$ mJy, the predicted sizes are in good agreement with the observational results. The late-type galaxies in our $S_{250} > 5$ mJy high-redshift sample have average disk radii of ~ 2.2 kpc. This is significantly larger than the mean disk size (~ 0.9 kpc) of all late-type galaxies in the same redshift range ($2 \leq z < 4$). However, the small mean disk size in case of all late-types is driven by the large number of dwarf galaxies. But even if we use the same stellar mass cut that the SPIRE 250 μm band selection induces, we find that the average size of the stellar

Figure 10. Predicted median cold gas mass vs flux in the PACS 160 and SPIRE 250 μm bands for galaxies selected at different redshifts. The green dotted vertical line shows a representative flux limit of the GOODS-N observations. The error bars show the 16th and 84th percentiles.
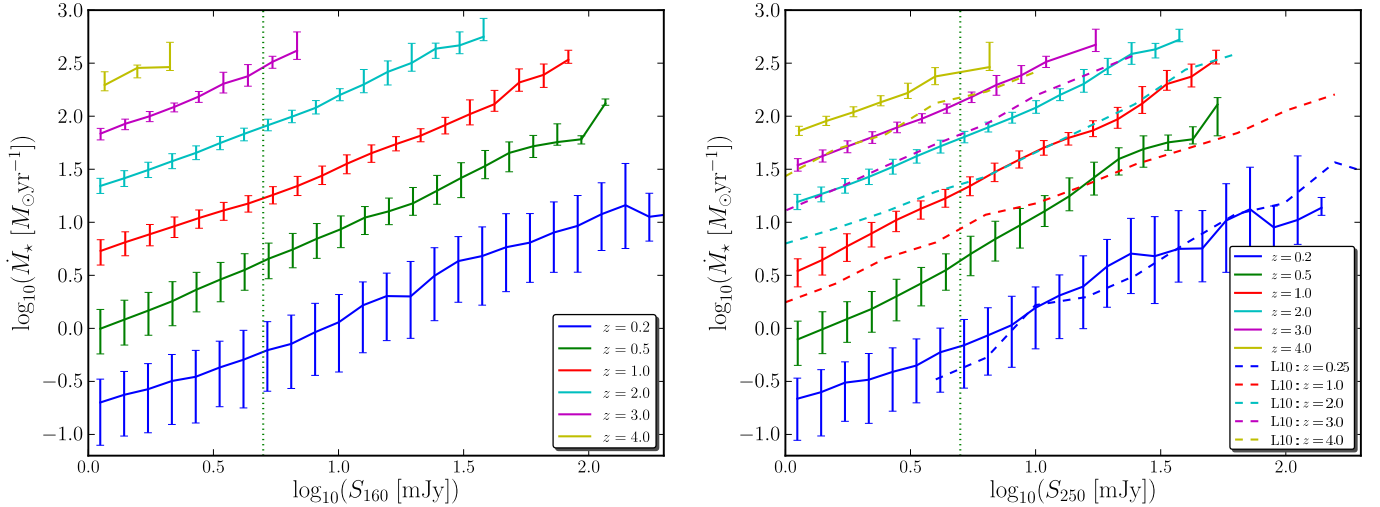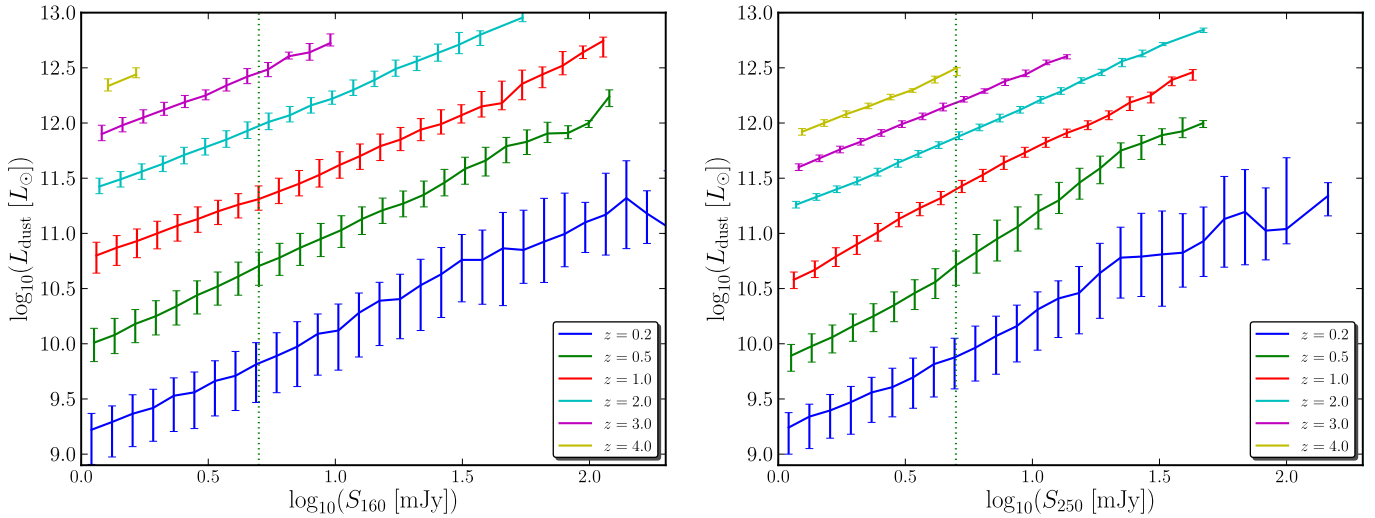

Figure 11. Predicted median star formation rate as a function of IR flux in the PACS 160 and SPIRE 250 μm bands at different redshifts. The green dotted vertical line shows a representative flux limit for the GOODS-N observations. The error bars show the 16th and 84th percentiles. The hatched lines on the right hand side plot (L10) are the predictions from Lacey et al. (2010).

disks is almost a factor of two smaller (~ 1.3 kpc) than the mean disk size of the high-redshift sample. Consequently, in our models, the IR bright late-type galaxies that have not experienced a merger within the last 500 Myr are on average larger than galaxies that emit lower SPIRE 250 μm fluxes. We speculate that this is because our models predict that larger galaxies are more gas rich, and we have already seen that there is a correlation between gas mass and IR luminosity. Our high-redshift sample of luminous IR galaxies also contains a few late-type galaxies whose stellar disks are > 7 kpc in size (for similar findings, see Rujopakarn et al. 2011).

4.2   Correlation with Merger Activity

Ultra-luminous galaxies in the local Universe are widely believed to be caused by major galaxy mergers (e.g. Sanders & Mirabel 1996; Colina et al. 2001; Farrah et al. 2003; Dasyra et al. 2006b; Väisänen et al. 2008). It has also been argued that ULIRGs will evolve into moderate-mass ellipticals (e.g. Genzel et al. 2001; Tacconi et al. 2002; Dasyra et al. 2006b) and/or AGN (Farrah et al. 2003, and references therein) after the merger or interaction. Merger driven star formation has also been studied using hydrodynamic simulations (e.g. Jog & Solomon 1992; Mihos & Hernquist 1996; Cox et al. 2008; Teyssier, Chapon & Bournaud 2010), which support the picture that massive starbursts could be driven by mergers. It has been argued (e.g. Dasyra et al. 2006a) that the majority of ULIRGs are triggered by almost equal-mass major mergers and that less violent mergers of mass ratio

Figure 12. Predicted median total IR luminosity ($L_{\rm dust}$) as a function of IR flux in the PACS 160 and SPIRE 250 μm bands at different redshifts. The green dotted vertical line shows a representative flux limit for the GOODS-N observations. The error bars show the 16th and 84th percentiles.
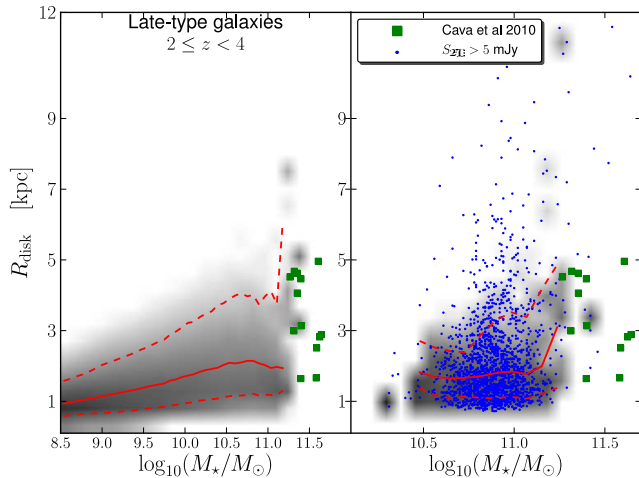

Figure 13. Hess plot of disk sizes ($R_{\rm disk}$) of the late-type galaxies as a function of stellar masses $M_\star$. All galaxies shown are in the redshift range $2 \leq z < 4$ and have not experienced a merger within the last 500 Myr. The right-hand panel shows only late-type galaxies that are brighter than 5 mJy in the SPIRE 250 μm band. The red lines show the median and 16 and 84 percentiles for simulated galaxies. The observed late-type galaxies, shown with green squares, are from Cava et al. (2010).

$< 1 : 3$ typically do not force enough gas into the nucleus to generate ULIRG luminosities. This is in agreement with simulations (e.g. Cox et al. (2008), but see also Teyssier, Chapon & Bournaud (2010) and references therein), although other factors (orbit, gas fraction, morphology) are also important. Even though some observations of IR luminous galaxies have failed to identify evidence for mergers, it has been argued that these highly obscured objects could be the end products of collisions between gas rich galaxies in a final phase of merger evolution (e.g. Auriere et al. 1996). Although this picture is well supported in the local Universe, the physical origin of ULIRGs at high redshift is less clear. For example, Sturm et al. (2010) identified two galaxies in early *Herschel*

observations that suggest that high redshift galaxies may be able to achieve LIRG and even ULIRG luminosities without experiencing mergers. Our model assumes that mergers can trigger bursts of star formation, but also incorporates the high gas accretion rates at high redshift predicted by cosmological simulations. It is therefore quite interesting to investigate what our model predicts for the fraction of luminous IR galaxies that are the result of mergers at high and low redshift.

To study the fraction of IR bright galaxies that are powered by mergers we record the time since the last merger $T_{\rm merger}$ or major merger $T_{\rm majormerger}$ for each galaxy in our simulation. "Minor" mergers are defined as those with a mass ratio[1] greater than 1:10, and "major mergers" as those with mass ratio greater than 1:4. Our model predicts that about 84 (53) per cent of high-redshift galaxies with $S_{160} > 10$ mJy have experienced a (major) merger during their lifetime. Note, however, that the fraction drops to about 34 percent if we concentrate on major mergers that have taken place less than 250 Myr ago, which are the mergers that are most likely to be causally linked to the star formation we are seeing. For the SPIRE 250 μm band, the results are very similar; about 86 (57) per cent of high-redshift galaxies with $S_{250} > 20$ mJy have experienced a (major) merger. If we again concentrate only on recent mergers in which the major merging event took place less than 250 Myr ago, the merger fraction drops to ~ 42 per cent. Thus our model makes an interesting prediction: roughly every second high-redshift ULIRG can achieve ULIRG luminosities without a recent major merger. This prediction differs from the findings of Gonzalez et al. (2010), who used a semi-analytic galaxy formation model (Baugh et al. 2005b) to study submillimetre galaxies (SMGs; $S_{850} > 5$ mJy). Gonzalez et al. (2010) finds that the majority of SMGs seen in current sub-mm surveys are starbursts triggered by major

---

[1] Here, the masses used in the ratio include stars, gas, and the dark matter within the optical radius of the galaxy, as in S08
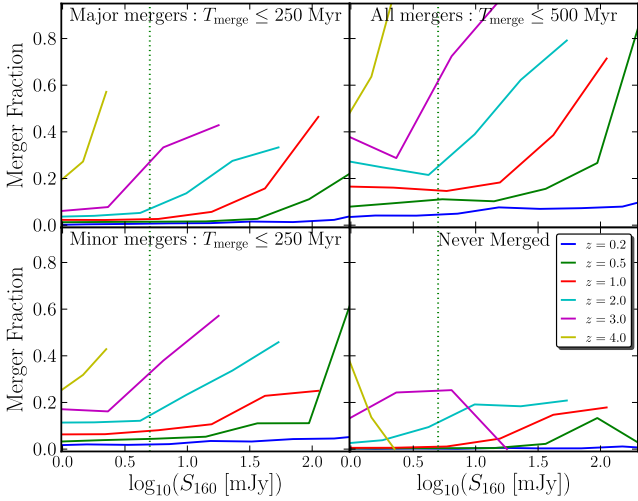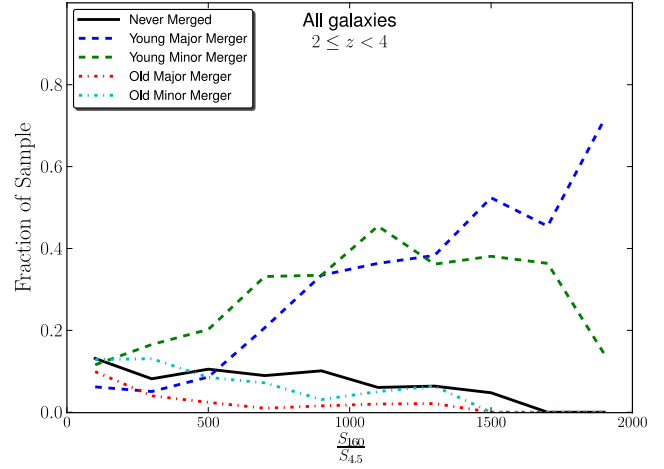
Figure 14. Merger fraction as a function of PACS 160 μm flux at different redshifts. The upper-left plot shows the recent major mergers, while the lower-left shows recent minor mergers (see text for definitions). The upper right panel shows the merger fractions as a function of PACS 160 μm flux for all mergers within the past 500 Myr, and the lower right panel shows the fraction of galaxies that have never merged. The vertical dotted line shows a representative flux limit for GOODS-*Herschel* (5 mJy).

Figure 15. The fraction of galaxies that have experienced a merger and that have never merged with another galaxy as a function of far- to mid-IR flux ratio. The flux ratio is the ratio between the PACS 160 and *Spitzer* IRAC 4.5 μm bands. The merger events have been divided into recent or young ($\leq$ 250 Myr) and less recent or old ($250 < T_{\mathrm{merger}} < 500$ Myr) and to minor and major incidents and are colour coded as given by the legend.

and minor mergers involving gas-rich disk galaxies (see also Baugh et al. 2005b).

We present these results in more detail in Figure 14, which shows the evolution of merger fractions as a function of PACS 160 μm flux at different redshifts. The upper-left plot shows that the merger fraction of recent (the latest merger took place less than or equal to 250 Myr ago) major mergers grows as a function of PACS 160 μm flux. This is true independent of studied redshift, although the steepest rise is noted at $z = 1$ and 4. The plot shows that the likelihood of the most luminous ULIRGs being powered by a merger is higher than for those that are less luminous. A similar trend can also be seen for minor mergers. This shows that under the right conditions, minor mergers may also trigger (U)LIRG-like activity. We note that Fig. 14 and the related results are qualitatively similar if instead of the PACS 160 μm flux we use the SPIRE 250 μm band.

We can use our models to attempt to identify observational quantities that could provide interesting indicators of starburst and merger activity for observations that are available or will become available soon. We wish to exploit the availability of extensive multi-wavelength data, from the rest UV to the FIR with *Herschel*, in fields such as GOODS. We focus on the redshift range $2 \leq z < 4$ for these experiments, and use the high redshift sample from our lightcones. It is reasonable to expect that starbursts will have high values of specific star formation rate (SSFR), $\dot{M}_\star M_\star^{-1}$. In a relatively narrow redshift range, we can use the ratio of a FIR flux to a Spitzer IRAC band as a proxy for SSFR.

Figure 15 shows the fraction of different types of mergers and the fraction of galaxies which have never merged as a function of far- to mid-IR flux ratio (colour). We choose to use the PACS 160 μm band as our far-IR band, because it is relatively close to the peak of the IR flux distribution in the studied redshift range ($2 \leq z < 4$), but at the same

time it suffers less from confusion than, e.g., the SPIRE 250 μm band. The mid-IR band chosen is the channel two of the *Spitzer* IRAC at 4.5 μm, which should provide a proxy for the stellar mass of a galaxy. Fig. 15 shows that our models predict that the probability that a galaxy has experienced a recent merger is a strong function of this far- to mid-IR flux ratio. For the most extreme values ($S_{160} S_{4.5}^{-1} \gtrsim 1300$) more than half of the galaxies have experienced a major merger within the last 250 Myr. We note that the results remain if we instead use other bands such as $S_{250} S_8^{-1}$ as the flux ratio. It will be interesting to test whether these IR colors are correlated with signatures of recent merger activity in observed galaxies.

We can also explore whether the use of a two colour diagram can provide further information. We expect that the rest-frame UV colours might correlate with the age of the starburst, and thus with the time since the merger event. We consider the filters of the Hubble Space Telescope's Advanced Camera for Surveys, because such data are available for GOODS. In Figure 16 we combine the information on UV-optical colour and far- to mid-IR flux ratio in a colour-colour plot. Again, we choose to use the PACS 160 μm band and IRAC's channel 2 (4.5 μm), because these channels allow the most robust comparison with observations of galaxies in the GOODS field. However, the results would be qualitatively similar with any IRAC channel or with the SPIRE 250 μm band. Fig. 16 shows that in our models, the most recent mergers are all located in the lower right region of each subplot, that is the region with the most extreme far- to mid-IR flux ratio and the bluest UV-optical colour.

The black contours indicate where the galaxies which have never merged are located and have been drawn using two dimensional Gaussian kernel density estimator. Note, however, that this region is also populated by recent mergers so we cannot conclude that the observed galaxies in this region have not experienced a recent merger. However, it is

interesting that there is a region of the diagram (shown by a green dotted line) in which all galaxies have experienced a recent merger. The functional form of the green line is as follows:

$$(F775W - F850lp)_{\mathrm{AB}} = A \log_{10} \frac{S_{160}}{S_{4.5}} + B \quad , \qquad (3)$$

where $A = 1$ and $B = -2.4$. Note, however, that this simple selection does not seem to be able to separate recent major mergers from less extreme mergers. If instead of the PACS we had used the SPIRE 250 μm band, the above equation would remain the same, but with $B = -2.7$.

It will be very interesting to test these predictions using surveys such as GOODS-*Herschel*, where multi-wavelength photometry as well as high resolution Hubble imaging are available. We plan to pursue this in a future work (Niemi et al. in prep).

5   SUMMARY AND CONCLUSIONS

In this work we made use of the semi-analytic models developed by S11, in which attenuation and re-emission of light by dust is modelled with a simple analytic approach, to make predictions for the physical and observable properties of galaxies that may be detected in deep fields by the *Herschel* Space Observatory. We used the semi-analytic models to generate mock lightcones resembling the GOODS survey but with 100 times the volume.

We first examined the differential number counts for galaxies in the PACS and SPIRE bands. We found very good agreement with the observed number counts derived from *Herschel* PACS data, for the overall counts and for galaxies binned by redshift at $z < 2$. At $z > 2$ our model underpredicts the number of more luminous galaxies in the PACS 100 and 160 μm bands. The agreement of our model predictions with the observed counts deteriorates as one moves to longer wavelengths, with increasingly poor agreement seen as one moves from PACS to SPIRE 250 μm and then to longer SPIRE bands. At 250 μm and longer wavelengths, the models tend to underpredict the number counts of intermediate flux galaxies ($10 \lesssim S_{250} \lesssim 100$ mJy), and overpredict the counts of brighter galaxies ($S_{250} \gtrsim 100$ mJy). We presented predictions using three different sets of empirical dust emission templates, and found interesting differences. However, it does not appear that any single simple modification to the dust templates could solve the discrepancies.

We discussed possible reasons for these discrepancies. These include uncertainties due to cosmic variance, possible evolution or scatter in the dust emission templates, a possible contribution to the IR light from obscured AGN, and the possibility that many of the bright sources are lensed. It is also possible that some of the physical processes in our model need revision, or that the stellar IMF was different in early galaxies, as has been suggested by Baugh et al. (2005b). However, our models produce reasonable agreement with the luminosity functions at rest-UV through NIR wavelengths, and with the observationally derived stellar mass functions and SFR functions at high redshift (see S11; Fontanot et al. 2009a, and references therein). Moreover, the top-heavy IMF model of Baugh et al. (2005b) that was developed to explain the observed sub-mm population at 850 μm does not appear to reproduce the SPIRE number counts particularly

well (Clements et al. 2010; Lacey et al. 2010), and does not produce enough galaxies with large stellar masses at high redshift (Swinbank et al. 2008). We also discuss the impact of flux boosting and blending on the observationally derived *Herschel* counts. This would explain why the discrepancy becomes larger with increasing wavelength, and might also be a larger effect for high redshift galaxies, which are compact and strongly clustered. A quick visual inspection of HST images for high redshift galaxies makes it clear that many, if not most, *Herschel* sources probably have contributions from multiple galaxies. Moreover, according to the simulations carried out by Rigby et al. (2011), more than half (~ 57 per cent) of sources detected at $\geq 5\sigma$ at 500 μm show a flux boosting by a factor > 1.5 and more than every fourth (~ 27 per cent) by a factor > 2. This is clearly a very serious issue when comparing theoretical predictions with these observations. We intend to use our simulations to create mock *Herschel* images, carry out the source detection procedure on these, and study the predicted effects of blending on the measured fluxes and galaxy counts. In addition, the *Herschel* team is working hard to better understand and overcome this problem.

With the resulting caveat that one probably cannot interpret our predicted *Herschel* fluxes as corresponding in a one-to-one fashion with directly observed *Herschel* fluxes (as currently available), but rather as intrinsic fluxes in the absence of blending, we used our model to make predictions for physical properties of *Herschel* detected galaxies. We showed the predicted relationships between PACS 160 and SPIRE 250 μm fluxes and stellar mass, halo mass, cold gas mass, SFR, and total IR luminosity as various redshifts. Our models show fairly strong trends between both S_{160} and S_{250} at a given redshift and all of these quantities except halo mass, which is quite flat as a function of both S_{160} and S_{250} at higher redshifts. This may have interesting implications for the clustering properties of these sources (for early observational results in GOODS South, see e.g. Magliocchetti et al. 2011). Our models predict that the galaxies that are likely to be detected in deep *Herschel* surveys such as GOODS-*Herschel* (S_{160} or $S_{250} > 5$ mJy) at high redshift ($z > 2$) have fairly large stellar masses ($M_\star \sim 6 \times 10^{10} - 3 \times 10^{11} \mathrm{M}_\odot$) and reside in fairly massive dark matter halos ($\gtrsim 10^{11} \mathrm{M}_\odot$). The latter is in good agreement with the minimum mass derived by Amblard et al. (2011) based on the observed clustering of SPIRE sources.

The simulated IR luminous galaxies were also found to be gas rich with cold gas masses ranging from $\sim 10^9$ up to $\sim 4 \times 10^{11} \mathrm{M}_\odot$. The bulk of the high redshift IR bright galaxies were found to contain $\sim 6 \times 10^{10} \mathrm{M}_\odot$ of cold gas. These predictions will soon be able to be tested with radio and mm observations such as those that will be obtainable with ALMA.

Our predicted stellar, cold gas, and halo masses at a given 250 μm flux are significantly higher than the corresponding predictions from the model of Lacey et al. (2010), which assumes a top-heavy IMF in starbursts. We show a quantitative comparison between our predicted SFR vs. S_{250} relation and that of Lacey et al. (2010), finding that although their predictions are similar to ours for low redshift galaxies, at higher redshift ($z \gtrsim 0.5$), their predicted SFR are lower than ours (at a given FIR flux) by about a factor of two.
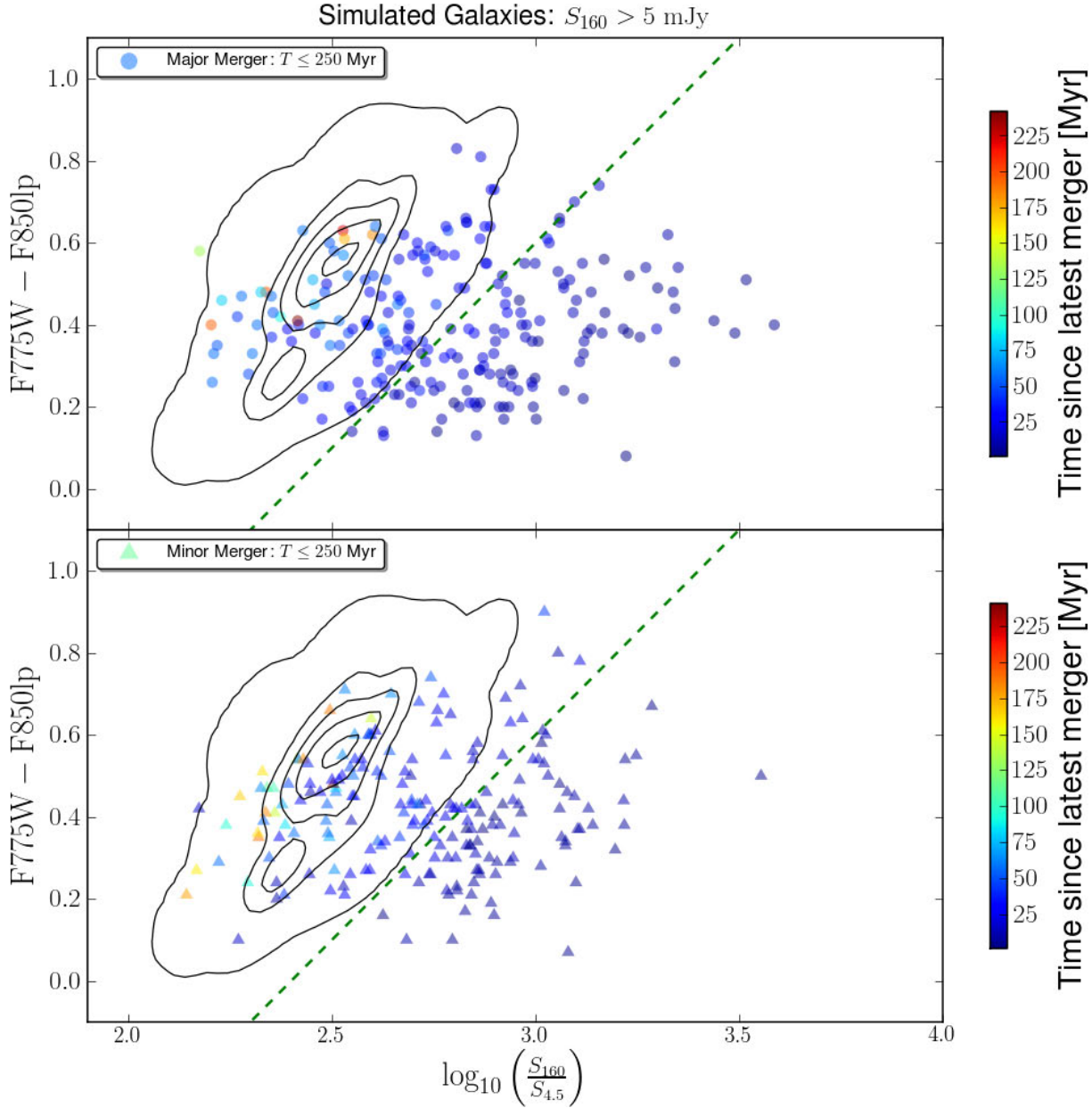
Figure 16. Rest-frame UV-optical colour as a function of far- to mid-IR flux. The flux ratio is the ratio between the PACS 160 and *Spitzer* IRAC 4.5 μm bands. The model galaxies have been colour coded by the time since the last merger in Myr. The green dotted line marks the region in which all simulated galaxies are recent mergers.

We investigated the radial sizes of high redshift ($2 \le z < 4$) late-type galaxies selected in the SPIRE 250 μm band and compared our predictions with the observations recently presented by Cava et al. (2010). We found that the SPIRE detectable galaxies are on average significantly larger than IR faint galaxies with comparable stellar masses. The mean disk size of IR luminous late-type galaxies was found to be in good agreement with the observations, although the statistics are extremely limited. We speculate that this is because larger galaxies are more gas rich and therefore more likely to be IR bright.

Finally, we investigated our model predictions for the importance of merger-driven starbursts in producing IR luminous galaxies at different redshifts. Although there is

clear evidence for a connection between merger activity and LIRGs and ULIRGs in the local Universe, the situation at high redshift is less clear. However, it has been suggested that an increasing fraction of LIRGs and ULIRGs at high redshift might not have a merger origin. We present quantitative predictions for the fraction of galaxies that have experienced a major or minor merger within a given timescale as a function of redshift and 160 μm flux. We find a fairly strong trend between the 160 μm flux and the probability that a galaxy has had a recent merger, indicating that brighter galaxies are more likely to be merger driven. However, we find the interesting result that in our models, a significant fraction (half or more) of IR-luminous galaxies at high redshift ($z > 2$) have not experienced a recent merger.

This implies that the high gas accretion rates and efficient feeding via cold flows predicted by cosmological simulations at high redshift can fuel a significant fraction of the galaxies detected by *Herschel*. This appears consistent with preliminary observational results (e.g. Sturm et al. 2010), but will be interesting to study and quantify in more detail in the near future.

In order to pursue this question further, we used our model to try to identify some observational photometric signatures associated with galaxies that have experienced recent mergers. We showed that there is a strong correlation between the mid-to-IR colour $S_{160}/S_{4.5}$ (PACS 160 μm to *Spitzer* IRAC channel 2 ratio) and the probability that a galaxy has had a recent merger. We also investigated a two color diagnostic using rest-frame UV colour and the 160 μm to IRAC 4.5 μm ratio. We found that recent mergers occupy a characteristic region of this diagram, suggesting another interesting observational tool to identify probable recent mergers. In a work in progress, we are making use of HST imaging in the GOODS-*Herschel* survey to study the morphologies of galaxies selected using these multi-wavelength diagnostics, in order to test our model predictions and the importance of merger-induced star formation at high redshift (Niemi et al., in prep).

REFERENCES

Almaini O., Lawrence A., Boyle B. J., 1999, MNRAS, 305, L59

Altieri B. et al., 2010, A&A, 518, L17

Amblard A. et al., 2011, Nature, 470, 510

—, 2010, Astronomy and Astrophysics, 518, L9

Auriere M., Hecquet J., Coupinot G., Arthaud R., Mirabel I. F., 1996, A&A, 312, 387

Baugh C. M., Lacey C. G., Frenk C. S., Granato G. L., Silva L., Bressan A., Benson A. J., Cole S., 2005a, Monthly Notices of the Royal Astronomical Society, 356, 1191

—, 2005b, MNRAS, 356, 1191

Berta S. et al., 2010, Astronomy and Astrophysics, 518, L30

Béthermin M., Dole H., Cousin M., Bavouzet N., 2010, Astronomy and Astrophysics, 516, 43

Blain A. W., Ivison R. J., Smail I., 1998, Monthly Notices of the Royal Astronomical Society, 296, L29

Bouwens R. J. et al., 2011, Nature, 469, 504

Brisbin D. et al., 2010, Monthly Notices of the Royal Astronomical Society, 409, 66

Bruzual G., Charlot S., 2003, Monthly Notices of the Royal Astronomical Society, 344, 1000

Calzetti D., 1997, Astronomical Journal v.113, 113, 162

—, 2001, The Publications of the Astronomical Society of the Pacific, 113, 1449

Cava A. et al., 2010, Monthly Notices of the Royal Astronomical Society: Letters, 409, L19

Chabrier G., 2003, The Publications of the Astronomical Society of the Pacific, 115, 763

Charlot S., Fall S. M., 2000, The Astrophysical Journal, 539, 718

Chary R., Elbaz D., 2001, ApJ, 556, 562

Chary R., Pope A., 2010, ArXiv e-prints

Clements D. L. et al., 2010, Astronomy and Astrophysics, 518, L8

Colbert J. W., Teplitz H., Francis P., Palunas P., Williger G. M., Woodgate B., 2006, The Astrophysical Journal, 637, L89

Colina L. et al., 2001, The Astrophysical Journal, 563, 546

Condon J. J., Huang Z.-P., Yin Q. F., Thuan T. X., 1991, ApJ, 378, 65

Conroy C., Gunn J. E., White M., 2009, The Astrophysical Journal, 699, 486

Cox T. J., Jonsson P., Somerville R. S., Primack J. R., Dekel A., 2008, MNRAS, 384, 386

Croton D. J. et al., 2006, Monthly Notices of the Royal Astronomical Society, 365, 11

Dale D. A., Helou G., 2002, The Astrophysical Journal, 576, 159

Dale D. A., Helou G., Contursi A., Silbermann N. A., Kolhatkar S., 2001, The Astrophysical Journal, 549, 215

Dasyra K. M. et al., 2006a, The Astrophysical Journal, 638, 745

—, 2006b, The Astrophysical Journal, 651, 835

Desert F.-X., Boulanger F., Puget J. L., 1990, Astronomy and Astrophysics (ISSN 0004-6361), 237, 215

Devriendt J. E. G., Guiderdoni B., 2000, A&A, 363, 851

Devriendt J. E. G., Guiderdoni B., Sadat R., 1999, A&A, 350, 381

Duc P.-A., Mirabel I. F., Maza J., 1997, A & A Supplement series, 124, 533

Dye S. et al., 2010, A&A, 518, L10

Eales S. et al., 2009, ApJ, 707, 1779

Elbaz D. et al., 2010, Astronomy and Astrophysics, 518, L29

Farrah D., Afonso J., Efstathiou A., Rowan-Robinson M., Fox M., Clements D., 2003, Monthly Notice of the Royal Astronomical Society, 343, 585

Farrah D. et al., 2007, The Astrophysical Journal, 667, 149

Floc'h E. L. et al., 2005, The Astrophysical Journal, 632, 169

Fontanot F., De Lucia G., Monaco P., Somerville R. S., Santini P., 2009a, MNRAS, 397, 1776

Fontanot F., Monaco P., Silva L., Grazian A., 2007, MNRAS, 382, 903

Fontanot F., Somerville R. S., 2010, ArXiv e-prints

Fontanot F., Somerville R. S., Silva L., Monaco P., Skibba R., 2009b, MNRAS, 392, 553

Genzel R. et al., 1998, Astrophysical Journal v.498, 498, 579

Genzel R., Tacconi L. J., Rigopoulou D., Lutz D., Tecza M., 2001, The Astrophysical Journal, 563, 527

Gilmore R. C., Somerville R. S., Primack J. R., Domínguez A., 2011, ArXiv e-prints

Glenn J. et al., 2010, MNRAS, 409, 109

Gonzalez J. E., Lacey C. G., Baugh C. M., Frenk C. S., 2010, eprint arXiv, 1006, 230

Goto T. et al., 2010, A&A, 514, 6

Granato G. L., Danese L., Franceschini A., 1997, Astrophysical Journal v.486, 486, 147

Granato G. L., Lacey C. G., Silva L., Bressan A., Baugh C. M., Cole S., Frenk C. S., 2000, The Astrophysical Journal, 542, 710

Griffin M. J. et al., 2010, A&A, 518, L3

Guiderdoni B., Hivon E., Bouchet F. R., Maffei B., 1998, MNRAS, 295, 877

Guiderdoni B., Rocca-Volmerange B., 1987, A&A, 186, 1

Guo Q., White S. D. M., 2009, MNRAS, 396, 39

Harwit M., Houck J. R., Soifer B. T., Palumbo G. G. C., 1987, ApJ, 315, 28

Hernán-Caballero A. et al., 2009, MNRAS, 395, 1695

Hopkins P. F. et al., 2009, Monthly Notices of the Royal Astronomical Society, 397, 802

Hopkins P. F. et al., 2009, MNRAS, 397, 802

Hughes D. H. et al., 1998, Nature, 394, 241

Hwang H. S. et al., 2010, Monthly Notices of the Royal Astronomical Society, 409, 75

Jog C. J., Solomon P. M., 1992, ApJ, 387, 152

Kennicutt R. C., 1989, ApJ, 344, 685

Kim D.-C., Sanders D. B., 1998, ApJS, 119, 41

Komatsu E. et al., 2009, ApJS, 180, 330

Lacey C. G., Baugh C. M., Frenk C. S., Benson A. J., Orsi A., Silva L., Granato G. L., Bressan A., 2010, Monthly Notices of the Royal Astronomical Society, 405, 2

Lacey C. G., Baugh C. M., Frenk C. S., Silva L., Granato G. L., Bressan A., 2008, MNRAS, 385, 1155

Lagache G., Dole H., Puget J.-L., 2003, Monthly Notice of the Royal Astronomical Society, 338, 555

Lagache G., Puget J.-L., Dole H., 2005, Annual Review of Astronomy and Astrophysics, 43, 727

Lagache G., et al., 2004, ApJS, 154, 112

Lapi A. et al., 2011, ArXiv e-prints

Leitherer C., Heckman T. M., 1995, Astrophysical Journal Supplement Series (ISSN 0067-0049), 96, 9

Lima M., Jain B., Devlin M., 2010, Monthly Notices of the Royal Astronomical Society, 406, 2352

Lima M., Jain B., Devlin M., Aguirre J., 2010, The Astrophysical Journal Letters, 717, L31

Lo Faro B., Monaco P., Vanzella E., Fontanot F., Silva L., Cristiani S., 2009, MNRAS, 399, 827

Lutz D., Spoon H. W. W., Rigopoulou D., Moorwood A. F. M., Genzel R., 1998, The Astrophysical Journal, 505, L103

Magdis G. E., Elbaz D., Hwang H. S., the PEP team, the HERMES team, 2011, eprint arXiv, 1102, 4236

Magliocchetti M. et al., 2011, ArXiv e-prints

Maraston C., 2005, Monthly Notices of the Royal Astronomical Society, 362, 799

Mihos J. C., Hernquist L., 1996, Astrophysical Journal v.464, 464, 641

Negrello M. et al., 2010, Science, 330, 800

Nguyen H. T. et al., 2010, Astronomy and Astrophysics, 518, L5

Oliver S. J. et al., 2010, Astronomy and Astrophysics, 518, L21

Pilbratt G. L. et al., 2010, A&A, 518, L1

Poglitsch A. et al., 2010, A&A, 518, L2

Reddy N. A., Erb D. K., Pettini M., Steidel C. C., Shapley A. E., 2010, ApJ, 712, 1070

Rieke G. H., Alonso-Herrero A., Weiner B. J., Pérez-González P. G., Blaylock M., Donley J. L., Marcillac D., 2009, ApJ, 692, 556

Rieke G. H., Low F. J., 1972, ApJ, 176, L95

Rigby E. E. et al., 2011, MNRAS, 415, 2336

Rigopoulou D., Spoon H. W. W., Genzel R., Lutz D., Moorwood A. F. M., Tran Q. D., 1999, AJ, 118, 2625

Robertson B., Bullock J. S., Cox T. J., Di Matteo T., Hernquist L., Springel V., Yoshida N., 2006, The Astrophysical Journal, 645, 986

Rowan-Robinson M., 2000, MNRAS, 316, 885

Rujopakarn W., Rieke G. H., Eisenstein D. J., Juneau S., 2011, The Astrophysical Journal, 726, 93

Sajina A. et al., 2008, The Astrophysical Journal, 683, 659

Sanders D. B., Mirabel I. F., 1996, Annual Review of Astronomy and Astrophysics, 34, 749

Sanders D. B., Scoville N. Z., Soifer B. T., 1991, ApJ, 370, 158

Sanders D. B., Soifer B. T., Elias J. H., Madore B. F., Matthews K., Neugebauer G., Scoville N. Z., 1988, ApJ, 325, 74

Silva L., Granato G. L., Bressan A., Danese L., 1998, ApJ, 509, 103

Somerville R. S., Gilmore R. C., Primack J. R., Dominguez A., 2011, ArXiv e-prints

Somerville R. S., Hopkins P. F., Cox T. J., Robertson B. E., Hernquist L., 2008, MNRAS, 391, 481

Somerville R. S., Kolatt T. S., 1999, MNRAS, 305, 1

Somerville R. S., Primack J. R., 1999, MNRAS, 310, 1087

Sturm E. et al., 2010, A&A, 518, L36

Swinbank A. M. et al., 2008, Monthly Notices of the Royal Astronomical Society, 391, 420

Tacconi L. J., Genzel R., Lutz D., Rigopoulou D., Baker A. J., Iserlohe C., Tecza M., 2002, The Astrophysical Journal, 580, 73

Teyssier R., Chapon D., Bournaud F., 2010, The Astrophysical Journal Letters, 720, L149

Tinsley B. M., Gunn J. E., 1976, Astrophysical Journal, 203, 52

Vaccari M. et al., 2010, A&A, 518, L20

Väisänen P. et al., 2008, MNRAS, 384, 886

Worthey G., 1994, The Astrophysical Journal Supplement Series, 95, 107

This paper has been typeset from a TEX/ LATEX file prepared by the author.